PRE- AND POST-BURNING ANALYSIS OF NANO-ALLUMINIZED PROPELLANTS. COMPARISON OF FOUR RUSSIAN NANO-Al POWDERS

Final Technical Report

by

Prof. Luigi De Luca and Prof. Luciano Galfetti

(December 2003 – December 2004)

United States Army

EUROPEAN RESEARCH OFFICE OF THE U.S. ARMY

London, England

CONTRACT NUMBER N62558-04-M-0303

Politecnico di Milano, Dipartimento di Energetica
Solid Propulsion Laboratory (SPLab)

Report Documentation Page

Form Approved
OMB No. 0704-0188

1. REPORT DATE	2. REPORT TYPE	3. DATES COVERED
DEC 2004	**N/A**	**-**

4. TITLE AND SUBTITLE
Pre- And Post-Burning Analysis Of Nano-Alluminized Propellants. Comparison Of Four Russian Nano-Al Powders

5a. CONTRACT NUMBER
5b. GRANT NUMBER
5c. PROGRAM ELEMENT NUMBER

6. AUTHOR(S)

5d. PROJECT NUMBER
5e. TASK NUMBER
5f. WORK UNIT NUMBER

7. PERFORMING ORGANIZATION NAME(S) AND ADDRESS(ES)
Politecnico di Milano, Dipartimento di Energetica Solid Propulsion Laboratory (SPLab)

8. PERFORMING ORGANIZATION REPORT NUMBER

9. SPONSORING/MONITORING AGENCY NAME(S) AND ADDRESS(ES)

10. SPONSOR/MONITOR'S ACRONYM(S)
11. SPONSOR/MONITOR'S REPORT NUMBER(S)

12. DISTRIBUTION/AVAILABILITY STATEMENT
Approved for public release, distribution unlimited

13. SUPPLEMENTARY NOTES
The original document contains color images.

14. ABSTRACT

Aluminum nano-powders of Russian production were examined and compared with the final goal to evaluate their application in solid rocket propellant formulations. A detailed investigation, concerning a compared characterization of differently sized aluminum powders, by BET (Specific Surface), EM (Electron Microscopy), XRD (X-Ray Diffraction), and XPS (X-ray Photoelectron Spectroscopy), expands the analysis already presented in the first interim report. A detailed investigation concerning a compared characterization of condensed combustion residues of several propellants, based on differently sized aluminum powders, expands the analysis presented in the second interim report. Experimental data concerning the ballistic characterization of several propellants, in terms of steady burning rates and other ballistic effects, expands the analysis already presented in the third interim report. Flame structures and agglomeration phenomena, at and near the burning surface, of several aluminized formulations were analyzed by high-speed, high-resolution, color, digital video recordings. All ballistic studies were performed at SPLab, Milan, Italy using industrial (for comparison) and laboratory composite solid rocket propellants based on ammonium perchlorate as oxidizer and HTPB as binder. The reference formulation was an AP/HTPB/Al composition with respectively 68/17/15 % mass fractions. Results obtained under a wide variety of operating conditions typical of rocket propulsion indicate, for increasing nano-Al mass fraction or decreasing nano-Al size, larger steady burning rates with essentially the same pressure sensitivity. A variety of other effects connected with nano-Al powders appears, depending on the details of the burning formulations. This first year report is focused on uncoated nano-powders of Russian production; the second year report (if continuation is approved) will deal with coated Russian nano-powders and US nanopowders. From a practical viewpoint, the actual properties of the available nominal Al have to be carefully checked before any actual use. With due precautions, nano-Al can be handled with safety in lab scale experiments, but extension to motor scale at this time is still an unknown.

15. SUBJECT TERMS					
16. SECURITY CLASSIFICATION OF:			17. LIMITATION OF ABSTRACT	18. NUMBER OF PAGES	19a. NAME OF RESPONSIBLE PERSON
a. REPORT **unclassified**	b. ABSTRACT **unclassified**	c. THIS PAGE **unclassified**	**SAR**	**51**	

Standard Form 298 (Rev. 8-98)
Prescribed by ANSI Std Z39-18

Abstract

Aluminum nano-powders of Russian production were examined and compared with the final goal to evaluate their application in solid rocket propellant formulations.

A detailed investigation, concerning a compared characterization of differently sized aluminum powders, by BET (Specific Surface), *EM* (Electron Microscopy), *XRD* (X-Ray Diffraction), and *XPS* (X-ray Photoelectron Spectroscopy), expands the analysis already presented in the first interim report.

A detailed investigation concerning a compared characterization of condensed combustion residues of several propellants, based on differently sized aluminum powders, expands the analysis presented in the second interim report.

Experimental data concerning the ballistic characterization of several propellants, in terms of steady burning rates and other ballistic effects, expands the analysis already presented in the third interim report.

Flame structures and agglomeration phenomena, at and near the burning surface, of several aluminized formulations were analyzed by high-speed, high-resolution, color, digital video recordings.

All ballistic studies were performed at SPLab, Milan, Italy using industrial (for comparison) and laboratory composite solid rocket propellants based on ammonium perchlorate as oxidizer and HTPB as binder. The reference formulation was an AP/HTPB/Al composition with respectively 68/17/15 % mass fractions. Results obtained under a wide variety of operating conditions typical of rocket propulsion indicate, for increasing nano-Al mass fraction or decreasing nano-Al size, larger steady burning rates with essentially the same pressure sensitivity. A variety of other effects connected with nano-Al powders appears, depending on the details of the burning formulations.

This first year report is focused on uncoated nano-powders of Russian production; the second year report (if continuation is approved) will deal with coated Russian nano-powders and US nanopowders.

From a practical viewpoint, the actual properties of the available nominal Al have to be carefully checked before any actual use. With due precautions, nano-Al can be handled with safety in lab scale experiments, but extension to motor scale at this time is still an unknown.

Table of Contents

(B) FINAL REPORT - THE FINAL REPORT SHALL INCLUDE A STATEMENT OF THE PROBLEM STUDIED, A SUMMARY OF THE MOST IMPORTANT RESULTS, A LIST OF ALL PUBLICATIONS AND TECHNICAL REPORTS PUBLISHED AND A LIST OF ALL PARTICIPATING SCIENTIFIC PERSONNEL SHOWING ANY ADVANCED DEGREES EARNED BY THEM WHILE EMPLOYED ON THE PROJECT. IT SHALL NOT BE DELAYED UNTIL REPRINTS OF PUBLICATIONS HAVE BEEN RECEIVED. IT IS NOT NECESSARY TO REPEAT TECHNICAL MATERIAL PREVIOUSLY PROVIDED IN AN INTERIM REPORT, BUT AN ABSTRACT OF NOT MORE THAN 300 WORDS, COVERING THE ENTIRE PERIOD OF PERFORMANCE, SHALL BE INCLUDED.

Nomenclature

Roman Symbols

a	= multiplicative factor in the Vieille steady burning rate law, *mm/s*
M_0	= propellant sample mass, *g*
M_0^{Al}	= Al content mass in the propellant sample, *g*
M^{res}	= mass of residues, *g*
M_{HCl}^{res}	= mass of residues after HCl treatment, *g*
p	= pressure, *bar*
r_b	= steady burning rate, *mm/*s

Greek Symbols

η^{res}	= % of oxide contained in the residues, relative to the total residues mass
ρ	= density, *g/cm*^{3}
ζ_{Al}^{res}	= % of Al mass contained in the propellant sample, found unburnt in the residues
$\zeta_{Al_2O_3}^{res}$	= % of Al mass contained in the propellant sample, used to form Al oxide in the residues
ζ^{res}	= $\zeta_{Al}^{res} + \zeta_{Al_2O_3}^{res}$; % of Al mass in the sample found in the residues (metal + oxide)

Abbreviations

BET	= Specific surface area measurement
CTEM	= Conventional Transmission Electron Microscopy
EDX	= Energy Dispersive X-Ray
EEW	= Electrical Explosion of Wires
HTEM	= High-Resolution Transmission Electron Microscopy
RAS	= Russian Academy of Sciences
SEM	= Scanning Electron Microscopy
TEM	= Transmission Electron Microscopy
TSU	= Tomsk State University
TPU	= Tomsk Polytechnical University
XPS	= X-Ray Photoelectron Spectroscopy
XRD	= X-Ray Diffraction

Part I INTRODUCTION

1. FINAL REPORT: STATEMENT OF WORK

According to the contract program, a series of aluminized composite propellants, manufactured including four nano-Al powders of Russian production, originated from different sources and produced with different techniques, was investigated. The baseline propellant is an AP/HTPB aluminized composition manufactured with:

- a nano-Al powder (type 01a, nominal size 0.1 μm) used in propellant P_01a;
- a micro-Al powder (type 05, nominal size 30 μm) used in propellant P_05;
- a mixed nano-Al powder (type 01a, nominal size 0.1 μm, 50%) and micro-Al powder (type 05, nominal size 30 μm, 50%) used in propellant P_BL_02.

The standard 30 μm Al powder is that traditionally used in solid rocket propellants formulated in western countries. The tested Al powders and relevant nomenclature are described in Table 1.1. Most of the propellant samples manufactured in the SPLab chemical laboratory are listed in Tables 5.1, 5.2, 5.3 and 5.4 (Part III, Sec. 5).

Aim of this part (first year) of the whole research program is to experimentally assess the influence of uncoated Al particle size on the ballistic properties of composite solid rocket propellants (steady burning rates, radiant ignition delays, ageing effects, burning surface characteristics, flame structure visualization, solid combustion residues, etc.).

2. ALUMINUM POWDERS UNDER INVESTIGATION

A wide range of Al powders, produced by a variety of international facilities (not always of commercial nature) with different techniques, is under examination; see Table 1.1 for a comprehensive summary. For sake of completeness, both nanometric (or ultra-fine) and micrometric (spheres or flakes) size ranges are investigated. Aluminum type 05 (spheres of 30 μm) is the standard Al powder traditionally used in solid propellant formulations in western countries, while Al type 06 (flakes of 50 μm characteristic dimension) is a cheap commercial product normally used for paints.

A well-known way to increase the reactivity of powders in general is to decrease their particle size. In fact, the reactivity of electroexplosive nanopowders increases with decreasing diameter during heating in air, as indeed shown by the observed decrease of oxidation onset temperature. Notice, however, that a protective film composed of non-stoichiometric aluminum oxides is typically formed when passivating, for example, by oxygen additives. Due to this fact, both the particle size and the content of metallic aluminum decrease for increasing specific surface (Fig. 2.1).

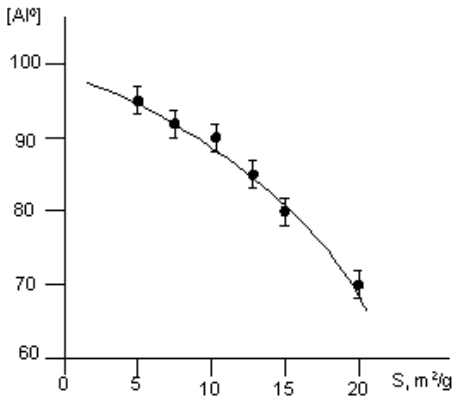

Fig. 2.1. Content of metallic aluminum depending on the particle diameter (EEW production).

3. AP/HTPB/Al SOLID PROPELLANT FORMULATION

Burning rate and radiant ignition delay measurements, high speed video-camera recordings, and residual combustion products analyses have been obtained for many aluminized propellant formulations (see Tables 5.1 – 5.4 in Section 5). All propellant formulations were designed and prepared in small batches, at most of 100 g, in the chemical laboratory of SPLab (Solid Propulsion Laboratory) of Politecnico di Milano. Propellants samples were thereafter manufactured, handled, and burned in a variety of specialized burners of SPLab.

Table 1.1 - Summary of Al powders under investigation
(this version supersedes previous ones).

Nomenclature	Source, Production Technique, and Size
Type 01	Source: Russia
Al_01a	EEW (similar to Alex); uncoated; nominal size: 0.10 μm; production 2002 ?
Al_01b (*)	EEW (similar to Alex); uncoated; large (0.30 μm); production summer 2004 ?
Al_01c (*)	EEW (similar to Alex); uncoated; small (<0.10 μm); production spring 2004 ?
Type 02	*Source: Russia (Institute of High Current Electronic, RAS)*
Al_02a	EEW; uncoated; nominal size: 0.17 μm; production: 2003
Al_02b	EEW; uncoated; nominal size: 0.17 μm; production: 2002
Al_02c	EEW; uncoated; nominal size: 0.17 μm; production: 1999
Type 03	*Source: Russia (TSU)*
Al_03a	Mechanical; uncoated; nominal size: 0.2 μm
Al_03b	Mechanical; uncoated; nominal size: 0.4 μm
Al_03c	Mechanical; uncoated; nominal size: 0.8 μm
Al_03d	Mechanical; uncoated; nominal size: 2.5 μm
Type 04	*Source: Russia*
Al_04a	Plasma condensation; coated; nominal size: 0.20 μm
Al_04b	Plasma condensation; coated; nominal size: 0.28 μm
Type 05	*Source: Italy (space industry supplier)*
Al_05	spherical; uncoated; nominal size: 30 μm
Type 06	*Source: Italy (commercial supplier)*
Al_06	flakes; uncoated; nominal size: 50 μm
Type 07	*Source: Russia*
Al_07 (*)	EEW (similar to Alex-L); coated; nominal size: 0.10 μm
Type 08	*Source: Russia (Institute of High Voltage Research, TPU)*
Al_08a (*)	EEW, coated; nominal size: < 0.10 μm; 3.5 g Jul 04
Al_08b (*)	EEW, coated; nominal size: < 0.10 μm; 100 g Sep 04
Type 09	*Source: USA*
Al_09 (*)	Plasma condensation; uncoated; nominal size: 0.04 μm

(*) : available but not yet investigated in this study.

Part II PRE-BURNING ANALYSIS

4. EXPERIMENTAL TECHNIQUES AND RESULTS

4.1 Pre-burning analysis: techniques

4.1.1 BET (specific surface area measurement)

The specific surface area is calculated from the nitrogen adsorption isotherm obtained by static volumetric measurement at liquid nitrogen boiling temperature (77 K).

All measurements reported have been carried out on a completely automated ASAP 2010 instrument from Micromeritics ® able to perform all pre-treatments and analyses as well as all calculations and regressions leading to the final determination of specific surface areas expressed in m^2/g (square meters per gram of sample), evaluated applying the BET algorithm to the nitrogen adsorption isotherm.

The Standard Methods ASTM D 4222-98 and ASTM D 3663-92 are addressed as reference for the measurement of the isotherm and for the application of the BET algorithm, respectively.

A vacuum system connected to a manifold able to perform outgassing and heat treatment as well as two gas supplies are required.

In particular, the following minimum requirements are recommended for the measurements:

- A vacuum system able to attain absolute pressure below 10^{-3} Torr;
- A constant volume pressure transducer in the range 0-1000 Torr with sensitivity of 0.1;
- A balance with 10^{-4} g sensitivity;
- Helium gas supply 99.9% purity;
- Nitrogen gas supply 99.9% purity;
- Fresh daily liquid nitrogen supply.

All samples have been outgassed at 100°C for at least 4 hours at absolute pressure < 10^{-3} Torr.

4.1.2 Electron Microscopy analysis (SEM and TEM)

Electron Microscopy characterization is able to describe the structure over many orders of dimensions, from the macroscopic to the atomic. Thanks to the increased resolution of modern instruments, the study of shape, dimension, morphology and defects has improved considerably. Scanning electron microscopy (*SEM*) and transmission electron microscopy (*TEM*) are used for the purpose; in the second case *TEM* is both conventional (*CTEM*) and high-resolution (*HREM*).

SEM microscope is a Cambridge Stereoscan 360 (maximum accelerating voltage: 40 kV) equipped with a LaB_6 filament with an ultimate resolving power of 3,5 nm. *CTEM* microscope is a Philips EM 300 (maximum accelerating voltage: 100 kV) equipped with a tungsten filament with a real resolving power of about 1 nm. *HREM* microscope is a Jeol JEM 2010 (maximum accelerating voltage: 200 kV) equipped with a LaB_6 filament with a nominal resolution of 0,18 nm.

In the *SEM*, specimens may be observed directly with little or no surface preparation, over useful magnifications ranging from approximately 20 to 100,000 times at a depth of field hundreds of times greater than that of the better light optical microscope used at high magnification and with monochromatic illumination. On the contrary, powder preparation for *TEM* is rather complicated owing to the need of obtaining films of about 100 nm thickness by means of an ultramicrotome. To ensure that the sample withstands the cutting process, without suffering extensive modification or damage, it is necessary to provide it with extra rigidity. This is usually accomplished in a process of embedding, which involves introducing the sample into a suitable medium such as an epoxy resin and then polymerizing it by gentle heating and/or by irradiation with ultraviolet light. Additives are often employed to speed the polymerization process and to vary plasticity and hardness of the end product in readiness for sectioning. The obtained sections are placed on a

copper folding grid of 100x200 meshes. In an attempt of reducing electrical charging of the samples (aluminum plus resin), ultramicrotomed films are coated by a thin evaporated carbon film before their observation in the electron microscope at room temperature.

4.1.3 X-Ray Diffraction analysis (XRD)

XRD spectra have been obtained to disclose the crystalline phases and their relative abundance. A qualitative analysis has been carried out by means of the standard powder method. In addition, a full-profile fitting procedure, based on the Rietveld method, allowed to perform very accurate quantitative analysis and to get complete structural refinements of each identified phase. Furthermore, by means of the investigation of the intrinsic broadening of diffraction peaks, accurate values of coherent scattering-domain lengths have been obtained too. XRD spectra were collected step-wise using Cu K_α radiation (λ=1.5416 Å) on a computer controlled Philips X'Pert PRO $\theta/2\theta$ diffractometer, equipped with a secondary curved pyrolytic graphite monochromator, in the 5-125° 2θ angular range, with 0.02° steps and 15 s counting time.

4.14 X-Ray Photoelectron Spectroscopy analysis (XPS)

XPS has been used, in addition to sputtering of Ar+ at 4 keV, to obtain chemical depth profiles that give information on the surface passivation layers and allow chemical species to be quantified. The sputtering rate has been estimated to be 5.5 nm/min. The spectrometer is a PHI-mod.5500, with monochromatized aluminum source for x-ray production. The spectra have been taken at 300 Watt.

4.1.5 Energy Dispersive X-Ray analysis (EDX)

This additional X-Ray based technique is useful to visualize the Al dispersion in the propellant bulk.

4.2 Pre-burning analysis: results

4.2.1 Specific surface area measurement (BET)

This technique, able to determine the specific surface area of a porous/powder material, has given information for sub-micrometric particles only. The samples having larger particles (Al_05 and Al_06) resulted non detectable. The following Table 4.1 summarizes the obtained data.

Table 4.1 - BET Specific Surfaces

	Nominal Size [μm]	Specific Surface [m^2/g]
Al_01a	0.10	15.6 ± 0.1
Al_02c	0.17	13.2
Al_03a	0.20	2.0
Al_03b	0.40	1.5
Al_03c	0.80	< 1 (sensitivity threshold)
Al_03d	2.5	< 1 (sensitivity threshold)
Al_05	30	< 1 (sensitivity threshold)
Al_06	50	< 1 (sensitivity threshold)

The inverse relationship of specific surface with particle size is evident.

In the following Fig. 4.1 the experimental adsorption isotherms are shown for all measured samples.

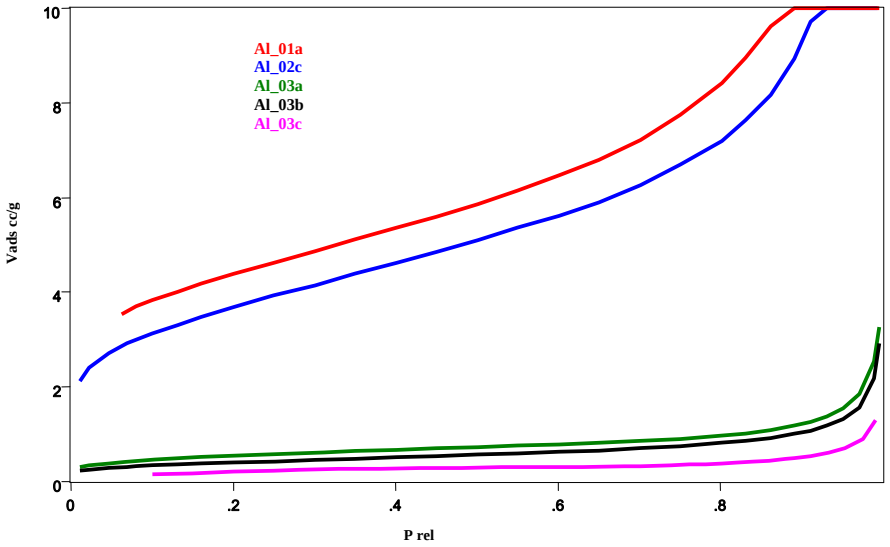

Fig. 4.1. Adsorption isotherms: adsorbed volume versus relative pressure.

From the curves of Fig. 4.1, the difference between the shape of the first two samples (Al_01a and Al_02c) and the remaining three ones (Al_03a, Al_03b, and Al_03c) is evident. In facts, the first two ones are typical of mesoporous materials with multilayer adsorption; while the second three ones are typical of non-porous materials with monolayer adsorption (Langmuir type). The substantial difference from the two families is related to the preparation technique: EEW leaves mesocavities in particle aggregates; mechanical milling leaves separated particles.

4.2.2 Electron Microscopy Analysis (SEM and TEM)

SEM micrographs are secondary electrons images of Al powder samples without any type of equipotential covering film.

Starting at a large scale (200 times - 1000 times), ALEX sample presents different types of irregular agglomerates of diameter up to 90 microns (Fig. 4.2a and 4.2b). At higher magnification (20.000 times - 50.000 times) it can be noticed that they are formed by primary spherical particles, whose diameter length is between 50 and 250 nm (Fig. 4.2c and 4.2d).

Sample Al_03-d reveals a completely spherical morphology of monodispersed particles at the largest scale (200 times -1000 times), whose dimensional range lies from 1 to 7 microns (Fig. 4.3a and 4.3b). Moreover, at higher magnification (10.000 times - 20.000 times) the absence of a nanometric structure inside spherical particles (Fig. 4.3c and 4.3d) appears evident.

Similar results are obtained for Al_05 sample: a more dispersed particle granulometry (from 1 to 70 microns) appears at the smaller scale (200 x - 1K x) (Fig. 4.4a and 4.4b); the shape is not as spherical as before and larger particles are present (from 1 to 70 μm). At higher magnification (10K x – 20K x) a compact morphology is visible with surface tracks and roughness (Fig. 4.4c and 4.4d).

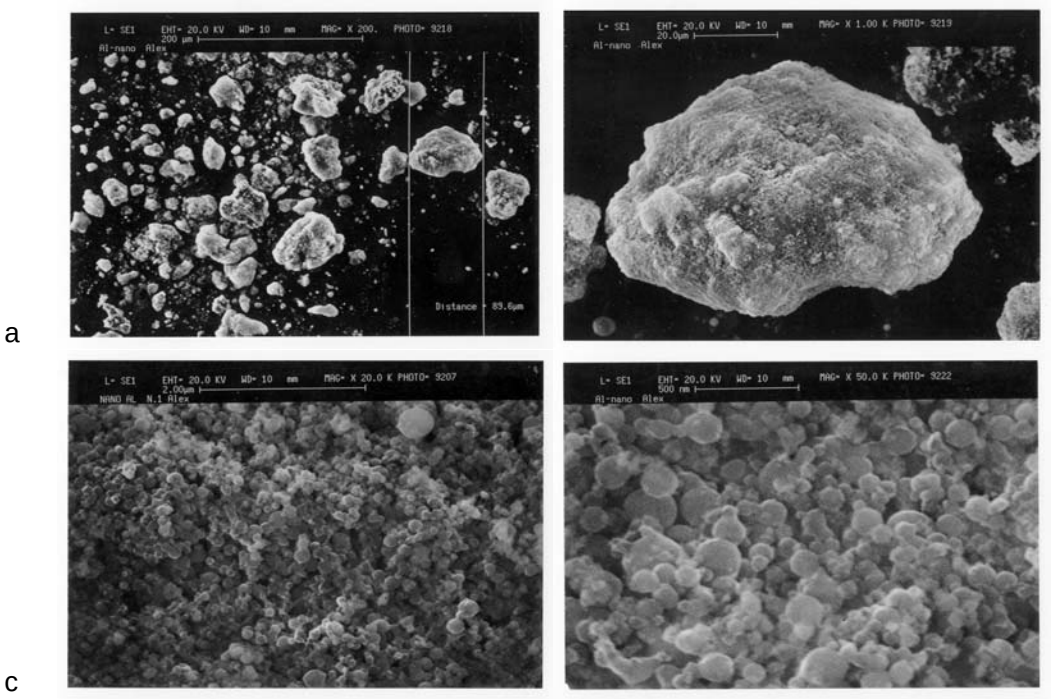

Fig. 4.2. SEM micrographs of Al_01a powder (similar to ALEX) at increasing magnifications: (a) 200 x; (b) 1K x; (c) 20K x; (d) 50K x.

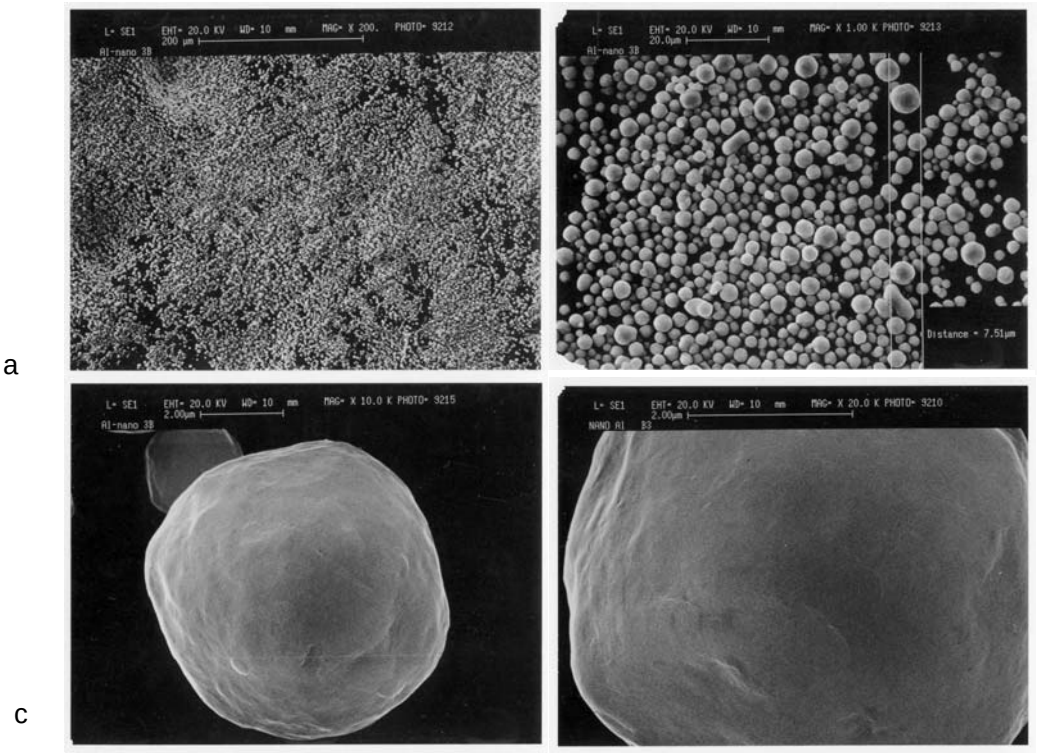

Fig. 4.3. SEM micrographs of Al_03d powder at increasing magnifications: (a) 200 x; (b) 1K x; (c) 10K x; (d) 20K x.

a

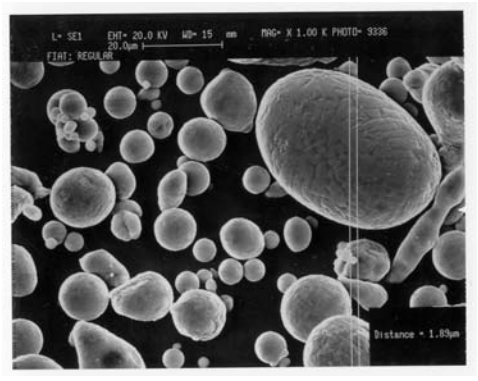

b

c

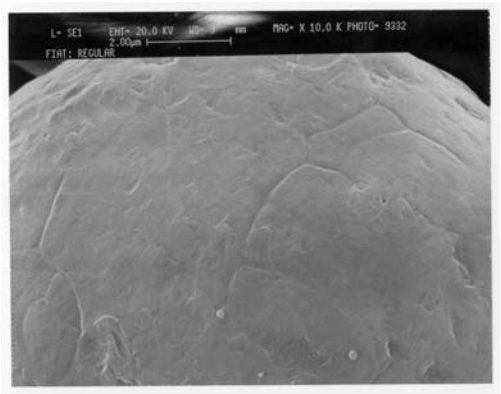

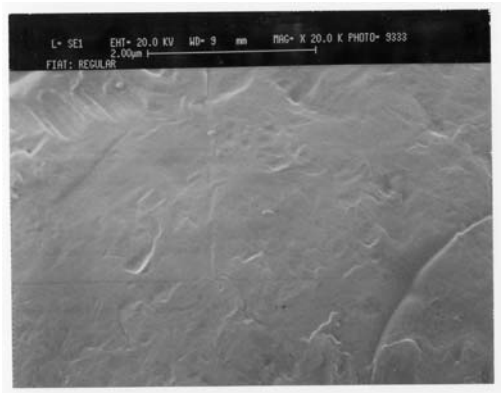

d

Fig. 4.4. SEM micrographs of Al_05 powder at increasing magnifications: (a) 200 x; (b) 1K x; (c) 10K x; (d) 20K x.

TEM micrographs are bright field images of ultrathin layers containing the dispersed powders. Aluminum domains are crystalline and, therefore, diffraction methods would be central to attempt an atomic-level structural characterization. For this purpose, different attempts are made to collect diffraction patterns from selected areas. Unfortunately beam damage represents a severe limitation for this purpose. In this way – notwithstanding the fading of the diffraction pattern – different crystalline orientations in the same area (polycrystals) are observed.

Starting from 20.000 times, ALEX sample shows a composite structure made of large particles (200-300 nm of diameter) mixed with very small and dispersed particles (down to 20 nm of diameter) (Fig. 4.5a). Smaller particle morphology varies from spherical to hexagonal shape. Spherical shapes suggest amorphous surfaces. Inside larger particles it is visible a inhomogeneous structure made of Al crystalline domain (darker) embedded in an amorphous matrix (brighter) (Fig. 4.5b); morphology of smaller particles appears spherical or exagonal (Fig. 4.5c and 4.5d).

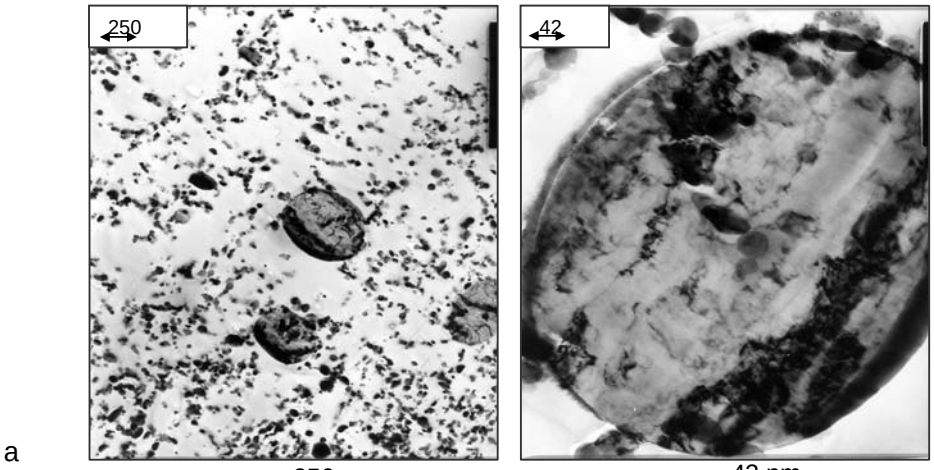

Fig. 4.5. TEM micrographs for Al_01 at different magnifications:
(a) bimodal size; (b) one of large particles; (c), (d) and (e) small particles with an hexagonal structure.

Uniformly dispersed micrometric particles of Al_03d powder are shown in Fig. 4.6a. They are larger than Al_01a ones, but show a similar internal structure (Fig. 4.6b). Particle dimension is typically about 1-7 μm, while in Al_01a the biggest ones are 200-300 nm.

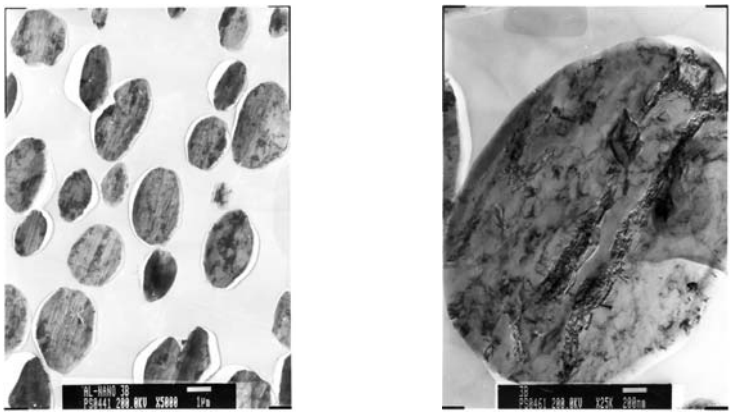

Fig. 4.6 - TEM micrographs for Al_03 at different magnifications:
(a) large particles; (b) a magnification showing metal (black) and oxide (grey) regions.

Fig. 4.7a and 4.7b show TEM micrographs of the Al_05 powder: the sizes of these particles are approximately double of the Al_03d powder particles. The morphology of Al_05 is quite similar to the previous one; but the particle shapes are more irregular and have larger dimensions. The same mixed composition (amorphous plus crystalline regions) is put in evidence for the internal structure. The largest extensions of dark Al domains are equivalent to the one measured by *XRD*.

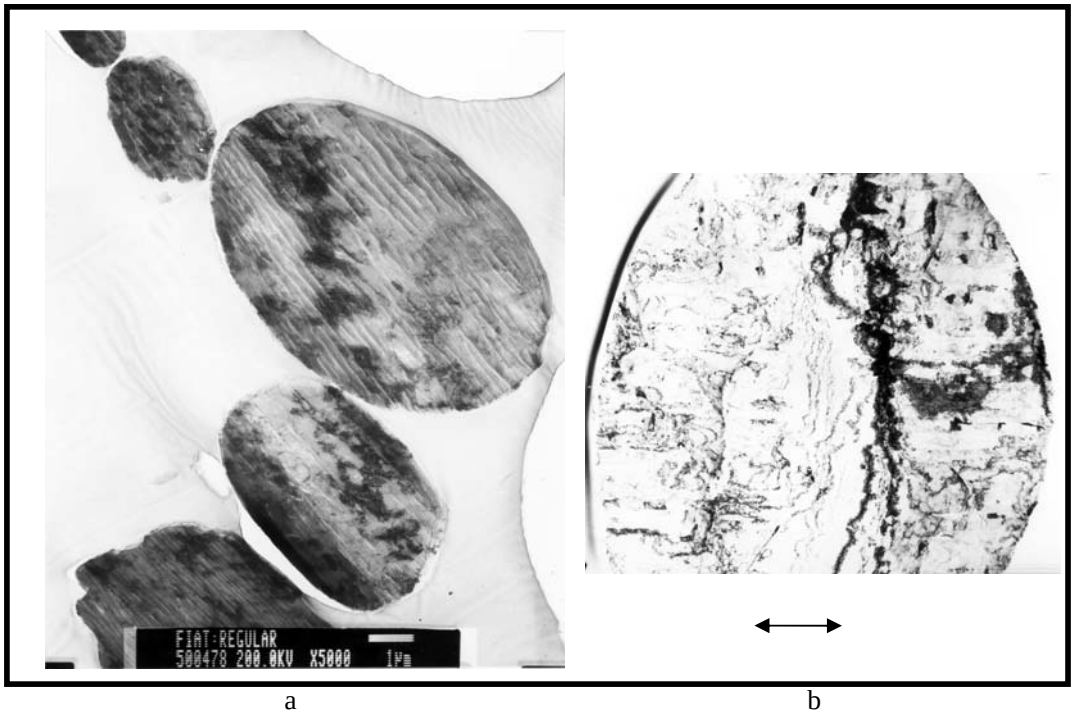

a b

Fig. 4.7. TEM micrographs for Al_05 at different magnifications: a) large particles; b) magnification showing metal (black) and oxide (grey) regions.

4.2.3 X-Ray Diffraction analysis (XRD)

The crystalline phases and their relative amounts, obtained by *XRD*, are shown in Table 4.2. As can be observed, all samples prepared by *EEW* contain two crystalline phases: the larger fraction is metallic-aluminum (Al > 90%), but a small fraction of aluminum nitride (AlN < 10%) is also present. On the contrary, samples obtained by other techniques only contain metallic-aluminum (100%) as crystalline phase.

The crystalline domain sizes (Φ) are also determined by XRD and they represent the maximum extension of ordered regions. Generally, this length is lower than particle size, because amorphous material can embed the crystals.

Powder Al_01a contains two crystalline phases: metallic-aluminum (Al 96.5%) and aluminum-nitride (AlN 3.5%). Their average crystalline domain lengths (Φ) are 130 nm and 20 nm, respectively. Samples of series Al_03 present an infinite length of crystalline domains, that means they are greater than 500 nm. Samples of Al_01 and Al_02 series show domains varying from 130 to 150 nm; while Al_05 shows 200 nm.

Table 4.2 - Crystalline phases determined by XRD technique.

Sample		Identified phases	
		Al	AlN
Al_01a	%	96.5	3.5
	Φ (nm)	130	20
Al_02a	%	95.5	4.5
	Φ (nm)	150	35
Al_02b	%	94.1	5.9
	Φ (nm)	140	32
Al_02c	%	92.2	7.8
	Φ (nm)	140	34
Al_03a	%	100	-
	Φ (nm)	∞	-
Al_03b	%	100	-
	Φ (nm)	∞	-
Al_03c	%	100	-
	Φ (nm)	∞	-
Al_03d	%	100	-
	Φ (nm)	98	-
Al_05	%	100	-
	Φ (nm)	200	-
Al_06	%	100	-
	Φ (nm)	∞	-

4.2.4 X-Ray Photoelectron Spectroscopy analysis (XPS)

XPS profiles allow to investigate atomic composition in a subsurface region, up to a depth of the order of hundreds of nanometers and to quantify the concentrations of main constitutive elements. Possible contaminations, at a concentration higher than 0.1 at. %, can also be detected by this technique. The quantitative analysis gives the atomic fraction of chemical elements, hydrogen excluded, so that the stoichiometric ratio and a chemical composition can be evaluated.

By considering the whole aluminium peak after each sputtering cycle, there is the possibility to decompose it in metallic-Al and oxidized-Al components, so that the relative amount of each component can be evaluated at different depths. These data represent the average on the sampled zone, that usually contains several single particles with the contribution of their native-oxide coatings. There is a relationship between the ratio Al_{met}/Al_{ox}, the oxide thickness "*s*" and the particle average diameter "*d*" as seen by the XPS probe:

$$Al_{met}/Al_{ox} = d / 2\, s$$

The knowledge of this ratio Al_{met}/Al_{ox} gives a lot of information concerning the metallic-particle size and the coating-oxide thickness that are present in the surface at different erosion times. In Table 4.3 the Al_{met}/Al_{ox} ratio is reported and it is clearly shown its variation with particle diameter.

The chemical depth profile of sample Al_01a is characterized by the presence of three main elements: Al, O, and N (Fig. 4.8). The relative atomic concentrations result constant in bulk after 7 min of sputtering, so suggesting a homogeneous composition with depth, typical for a system made of particles much smaller than the analysed area. The concentration values are: total-Al 64 at%; O 32 at%; N 2 at%. The aluminium amount can be separated, by Al-peak decomposition, in metallic-Al and oxidised-Al, at different sputtering time (Fig. 4.9, from bottom to top are: surface, after 3 min, after 7 min). By decomposing the Al peak, and by considering the presence of a small percentage of AlN (2 at%), the total-Al splits in 38 at% of metal-Al and 24 at% of oxidized-Al. Iron and molibdenum contamination have also been detected at very low concentrations (< 1 at%) in bulk. The surface transition region, represented by a thin coating of prevailing aluminum oxide, is estimated to be about 30 nm thick. A value close to 1.5, for the ratio $O/Al_{ox,}$ suggests that the Al-oxide is stoichiometric Al_2O_3.

Table 4.3 - XPS atomic concentrations per unit volume
(data are taken after 12 min sputtering = about 60 nm)

Atomic %	O	Al	N	O/Al_{ox}	Al_{met}/Al_{ox}
Al_01	33 (± 2)	63 (± 4)	2 (± 1)	1.3	1.6
Al_02a	35	62	2	1.2	1.1
Al_02b	35	62	2	1.3	1.2
Al_02c	46	51	3	2.0	1.3
Al_03a	15	85	-	0.9	3.8
Al_03d	22	78	-	1.4	3.8
Al_05	12	88	-	0.9	5.6
Al_06	12	86	-	1.4	11.0

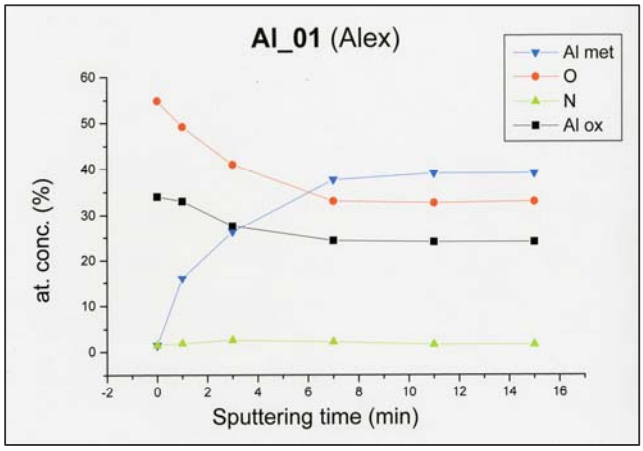

Fig. 4.8. XPS profiles of atomic composition. Powder: Al_01.

Chemical depth profiles of samples Al_02 are also characterized by the presence of the same three elements: Al, O, and N (Fig. 4.10a, b and c). The relative atomic concentrations result almost constant in bulk after sputtering. The most important observation is that oxygen concentration seems to increase with the age of the sample (from 35 at% for 2003 to 46 at% for 1999), as can be observed in Tab. 4.3. It is also noticeable that the profiles of samples prepared in 2002 and 2003 are quite similar (O 35 at%; Al 62 at%), while the one prepared in 1999 shows an increased oxygen (O 46 at%) that masks the signal of aluminium (Al 51 at%). As the Alox did not increased with oxygen in sample Al_02c, it can be deduced that sample prepared in 1999 is more hydrated that the other two (see Table 4.3). The concentration of nitrogen is around 2 at% for all the three samples.

Chemical profiles obtained from the series Al_03, prepared by mechanical mixing, never show the presence of nitrogen, because AlN is formed only under severe conditions. In these cases particles are larger and the contribution of metal-Al becomes more evident, this is because the relative amount of surface oxide in the analysed volume is diminished with respect to bulk material. In facts, the oxygen and aluminium amounts, in the same volume, are very different from samples of series Al_01 and Al_02 (as summarized in Tab. 4.3). Moreover, while at the external surface the ratio O/Alox appears to be around 2 (mixing oxide-hydroxide), in the bulk the ratio O/Alox is 1, thus suggesting the presence of substoichiometric oxide at particle surfaces. No difference have been appreciated in changing from 0.2 to 2.5 microns of nominal size (Figs. 4.11a and 4.11b).

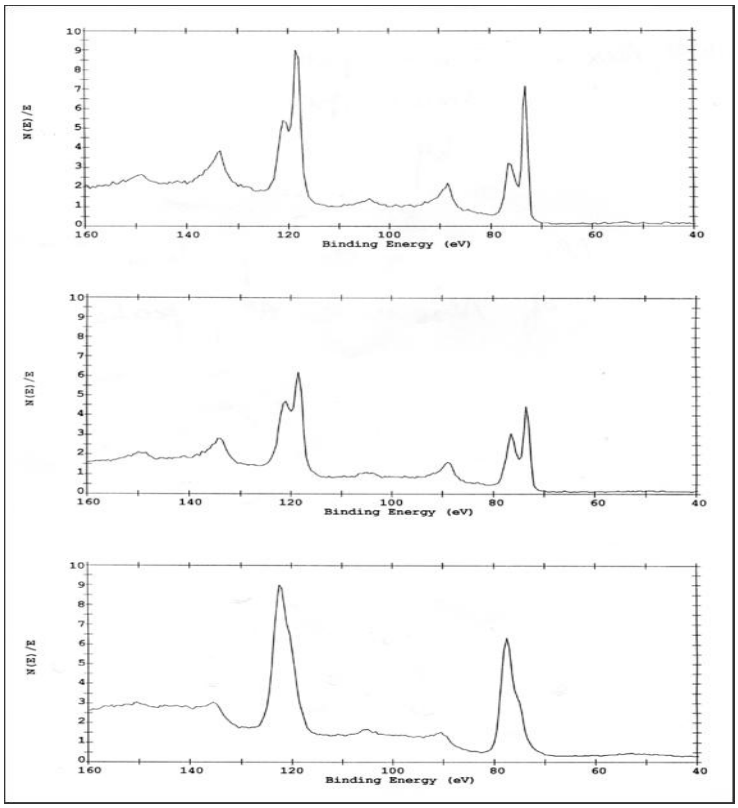

Fig. 4.9. XPS profiles of Al_01 powder at three different sputtering times.

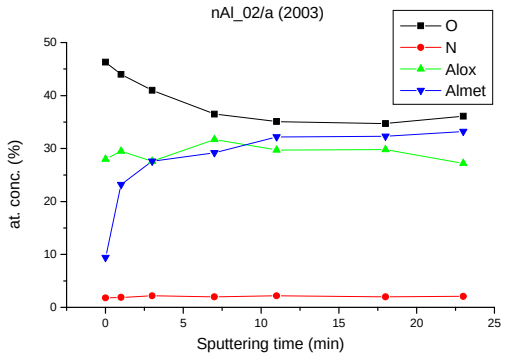

Fig. 4.10a. XPS profiles of atomic composition. Powder: Al_02a.

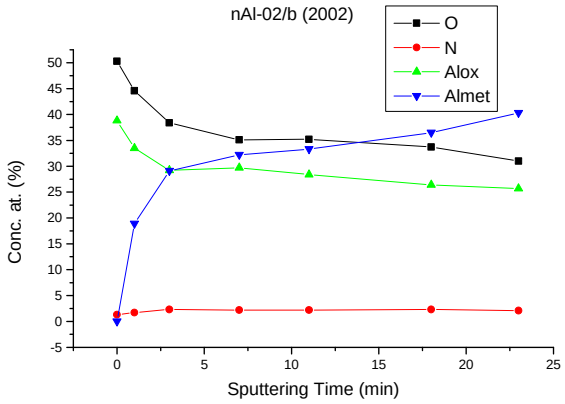

Fig. 4.10b. XPS profiles of atomic composition. Powder: Al_02b.

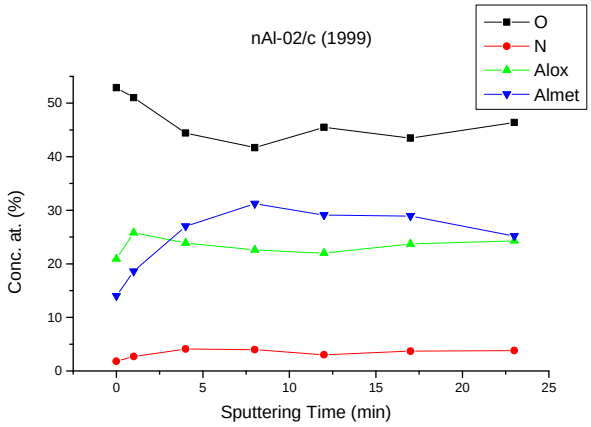

Fig. 4.10c. XPS profiles of atomic composition. Powder: Al_02c.

The profile of sample Al_05, shown in Fig. 4.12, results to be similar to the ones of series Al_03; in facts, metal-Al is the prevailing element even at higher concentration (see Tab. 4.3). Moreover, the ratio O/Alox is 2 (mixing oxide-hydroxide) at the external surface and 1 in bulk, as before.

Also the profile of sample AL_06 results to be similar to the previous ones; metal-Al is the prevailing element and the ratio O/Alox tends to reach 1 in bulk. In this case, a small amount (around 1 at. %) of metallic iron is detected at the surface, under the thin native oxide.

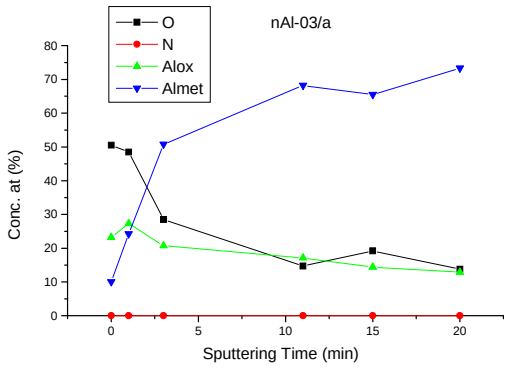

Fig. 4.11a. XPS profiles of atomic composition. Powder: Al_03a.

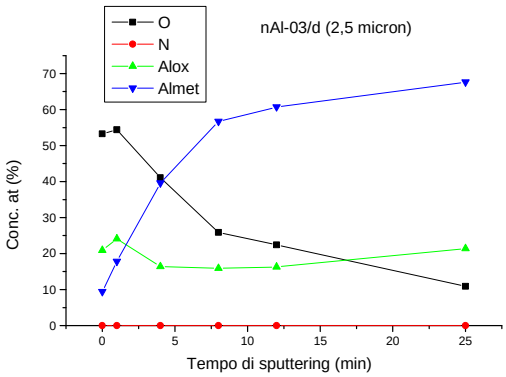

Fig. 4.11b. XPS profiles of atomic composition. Powder: Al_03d.

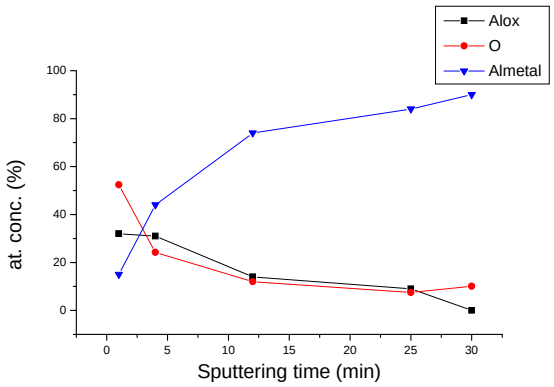

Fig. 4.12. XPS profiles of atomic composition. Powder: Al_05.

4.2.5 Energy Dispersive X-Ray analysis (EDX)

Representative results visualizing the Al dispersion in the propellant matrix are reported in Fig. 5.1.

Part III BURNING RATE AND FLAME VISUALIZATION

5. STEADY BURNING RATE MEASUREMENTS

5.1 Tested formulations

5.1.1 AP/HTPB/Al Reference Formulation

To investigate the ballistic effects connected with nano-Al, contrasting in particular the effects of nanometric vs. micrometric Al powders, a reference composite formulation consisting of 68% ammonium perchlorate (AP), 17% HTPB binder, and 15% aluminum (Al) was selected.

5.1.2 Main Ingredients

Different propellant compositions were tested according to the above basic formulation and using the ingredients described in next section.

- As oxidizer only AP has been used, provided for practical reasons by two different suppliers: AP-1 from a propulsive supplier and AP-2 from a commercial supplier.
- As metallic fuel, the wide range of Al powders listed in Table 1 is under test; but in this report attention is mainly focused on nanometric uncoated aluminum particles of Russian production.
- The binder typically employed is the common Hydroxyl-Terminated PolyButadiene – DiOctilAdipate - IsoPhorone-DIsocyanate (HTPB – DOA - IPDI). In general HTPB R-20 has been used; occasionally, other hydrocarbon binders have also been used.

Thus, all tested compositions contain 83% mass fraction of solids and may differ for the supplier and size distribution of AP particles (monomodal vs. bimodal but always for a total mass fraction of 68%); nature and size distribution of Al particles (monomodal vs. bimodal but always for a total mass fraction of 15%); nature of the binder (but always for a total mass fraction of 17%). Bimodal AP size distributions are based on a coarse/fine ratio of 4 (c/f = 4): coarse particles (80%) in the range 150 $\pm$ 10 µm and fine particles (20%) in the range 75 $\pm$ 5 µm. Monomodal AP size distributions only include particles in the range 70-80 µm. Bimodal Al size distributions are based on a mixture on micrometric (coarse) and nanometric (fine) particles with parametrically variable c/f ratio: coarse particles are typically in the range 30-50 µm and fine particles in the range 0.1-0.2 µm.

5.1.3 Basic Formulation and Variants

Out of the several dozens of compositions tested, a few selected AP/HTPB/Al propellant series are discussed in this report (Tables 5.1 – 5.4). Series I is meant to contrast the effects of micro-Al type 06 replaced by the same amount of uncoated nano-Al (mainly of type 02b, see Table 5.1). This series includes seven Al compositions between the two bracketing formulations P_06 and P_02b respectively consisting of 100% micro-Al flakes and 100% nano-Al particles. The remaining five propellants of Series I (P_07_B01a, P_07_B02b, P_07_B03d, P_08, P_09) feature a bimodal Al distribution, with coarse (50 or 30 µm) and ultra-fine (usually 0.17 µm) particle sizes, according to the indicated c/f ratio. All propellants of series I (and II as well) employ a bimodal size distribution (c/f = 4) of AP-2 as oxidizer (from a commercial supplier) and HTPB R-20 as binder.

Series II is meant to assess how burning rate scales with Al particle size and thus includes only monomodal Al distribution (see Table 5.2). Propellant P_05 includes 100% of the micro-Al type 05 used in propulsive applications (spheres of 30 µm diameter). Propellant P_03d includes Al particles of 2.5 µm nominal size; propellant P_04a includes Al particles of 0.2 µm nominal size and protected by a hydrocarbon coating; propellant P_01a includes Al particles of 0.1 µm nominal size and very similar to the commercial Alex product. To allow a meaningful comparison of both effects, a common baseline propellant (called P_06) has been enforced for both series I and II. Propellant P_06 include 100% of micro-Al type 06, a low-cost commercial product. All propellants of series II (and I as well) employ a bimodal size distribution (c/f = 4) of AP-2 as oxidizer (from a commercial supplier) and HTPB R-20 as binder.

In Series III (Table 5.3), specific effects regarding the nano-Al types under test were systematically investigated using a bimodal size distribution (c/f = 4) of AP-1 as oxidizer (from a propulsive industry supplier) and HTPB R-20 as binder .

Details of the formulation ingredients concerning the oxidizer and binder were investigated in propellant Series IV (Table 5.4). In this series, specific burning tests were conducted with several AP-1 (instead of AP-2) grain size distributions and a different HTPB binder (R-45 instead of R-20).

Table 5.1 - First series of propellant formulations: bimodal AP-2 (20% fine + 80% coarse), monomodal or bimodal Al, HTPB R-20 binder.

Propellant Short Notation	AP supplier and granulometry (µm)	Al (15%)		Binder (17%)
		Type	nominal size	
P_06	AP-2; 70-80, 140-160	100% type 06	50 µm	HTPB R-20
P_07_B01a	AP-2; 70-80, 140-160	80% type 06 20% type 01a	50 µm 0.10 µm	HTPB R-20
P_07_B02b	AP-2; 70-80, 140-160	80% type 06 20% type 02b	50 µm 0.17 µm	HTPB R-20
P_07_B03d	AP-2; 70-80, 140-160	80% type 06 20% type 03d	50 µm 2.5 µm	HTPB R-20
P_08	AP-2; 70-80, 140-160	50% type 06 50% type 02b	50 µm 0.17 µm	HTPB R-20
P_09	AP-2; 70-80, 140-160	50% type 05 50% type 02b	30 µm 0.17 µm	HTPB R-20
P_02b	AP-2; 70-80, 140-160	100% type 02b	0.17 µm	HTPB R-20

Table 5.2 - Second series of propellant formulations: bimodal AP-2 (20% fine + 80% coarse), monomodal Al, HTPB R-20 binder.

Propellant Short Notation	AP supplier and granulometry (µm)	Al (15%)		Binder (17%)
		Type	nominal size	
P_06	AP-2; 70-80, 140-160	100% type 06	50 µm	HTPB R-20
P_05	AP-2; 70-80, 140-160	100% type 05	30 µm	HTPB R-20
P_03d	AP-2; 70-80, 140-160	100% type 03d	2.5 µm	HTPB R-20
P_04a	AP-2; 70-80, 140-160	100% type 04a	0.2 µm	HTPB R-20
P_01a	AP-2; 70-80, 140-160	100% type 01a	0.1 µm	HTPB R-20

Table 5.3 - Third series of propellant formulations: bimodal AP-1 (20% fine + 80% coarse), bimodal Al, HTPB R-20 binder.

Propellant Short Notation	AP supplier and granulometry (µm)	Al (15%)		Binder (17%)
		Type	nominal size	
P_Al_01a	AP-1; 70-80, 140-160	80% type 05 20% type 01a	30 µm 0.1 µm	HTPB R-20
P_Al_02a	AP-1; 70-80, 140-160	80% type 05 20% type 02a	30 µm 0.17 µm	HTPB R-20
P_Al_02b	AP-1; 70-80, 140-160	80% type 05 20% type 02b	30 µm 0.17 µm	HTPB R-20
P_Al_02c	AP-1; 70-80, 140-160	80% type 05 20% type 02c	30 µm 0.17 µm	HTPB R-20
P_Al_03a	AP-1; 70-80, 140-160	80% type 05 20% type 03a	30 µm 0.2 µm	HTPB R-20
P_Al_03b	AP-1; 70-80, 140-160	80% type 05 20% type 03b	30 µm 0.4 µm	HTPB R-20
P_Al_03c	AP-1; 70-80, 140-160	80% type 05 20% type 03c	30 µm 0.8 µm	HTPB R-20
P_Al_03d	AP-1; 70-80, 140-160	80% type 05 20% type 03d	30 µm 2.5 µm	HTPB R-20
P_Al_04a	AP-1; 70-80, 140-160	80% type 05 20% type 04a	30 µm 0.20 µm	HTPB R-20
P_Al_04b	AP-1; 70-80, 140-160	80% type 05 20% type 04b	30 µm 0.28 µm	HTPB R-20

Table 5.4 – Fourth series of propellant formulations: monomodal or bimodal AP-1 (20% fine + 80% coarse), monomodal or bimodal Al, HTPB R-20 or HTPB R-45 binder.

Propellant Short Notation	AP supplier and granulometry (µm)	Al (15%)		Binder (17%)
		Type	nominal size	
P_BL_05	AP-1; 70-80, 140-160	100% type 05	30 µm	HTPB R-20
P_BL_01	AP-1; 70-80, 140-160	100% type 01a	0.1 µm	HTPB R-20
P_BL_02	AP-1; 70-80, 140-160	50% type 01a 50% type 05	0.1 µm 30 µm	HTPB R-20
P_BL_01a	AP-1; 80-140	100% type 01a	0.1 µm	HTPB R-20
P_BL_02a	AP-1; 80-140	50% type 01a 50% type 05	0.1 µm 30 µm	HTPB R-20
P_BL_01c	AP-1; 80-140	100% type 01a	0.1 µm	HTPB R-45
P_BL_02b	AP-1; 80-140	50% type 01a 50% type 05	0.1 µm 30 µm	HTPB R-45

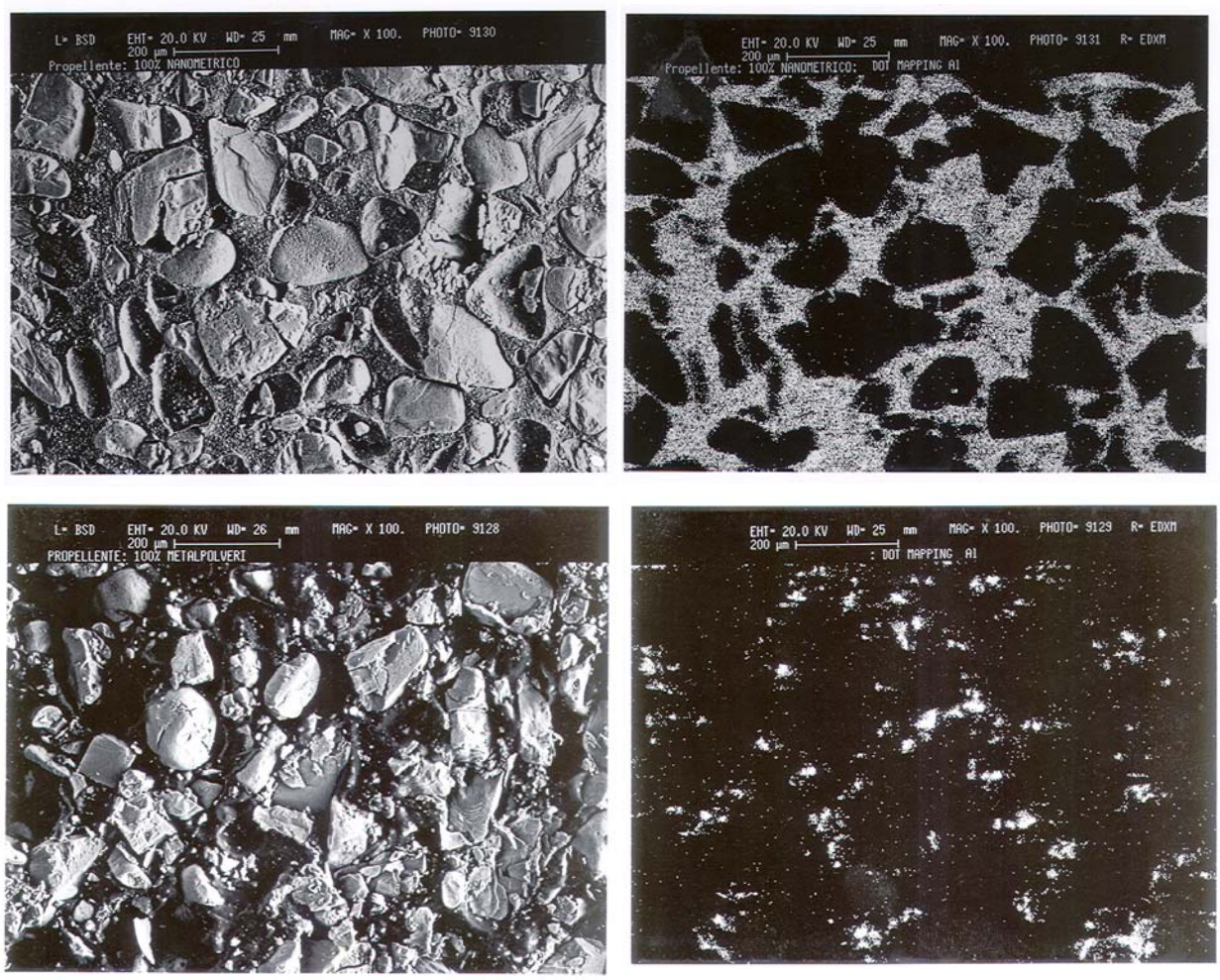

Fig. 5.1. Visualization of the propellant interparticle microstructure or binder matrix: nanometric Al (upper pictures) and micrometric Al (lower pictures). SEM images on the left, EDX images on the right. Propellant of series I (see Table 5.1).

5.1.4 Propellant Texture (interparticle matrix)

Filling of the propellant interparticle microstructure or binder matrix (the fine material distributed among the coarse oxidizer particles) appears of much better quality (uniform and well-distributed) in the case of nanometric Al, see Fig. 5.1 upper pictures, rather than in the case of micrometric Al, see Fig. 5.1 lower pictures. The microstructure material includes binder (HTPB R-20), Al particles, and also the smallest AP particles making the oxidizer mass fraction. In both cases, the coarse oxidizer grains (bimodal AP-2) of irregular shape are well visible under SEM analysis; EDX imaging was instead used to reveal the Al distribution. Each picture includes in its upper strip a mark for the 200 µm scale.

5.1.5 Handling and Safety Remarks

Aluminum nano-powders used in this experimental investigation are naturally protected by a thin layer of aluminum oxides which makes possible their handling without inadvertent ignition. This protective layer preserves the metal from additional oxidation but the powder may be easily attacked by water, basic and acid solutions, with hydrogen development in the environment.

Fire and explosions are potentially deadly risks in any process involving powder operation, notwithstanding the reduced chemical reactivity of the used nano-Al powders. Moreover aluminum powder is harmful if inhaled, causes irritation to eyes and respiratory tract. All precautions have been taken to prevent such risks. The powder was stored in a well closed container at a temperature of 4-10 °C. Handling of aluminum powder was made in the presence of a stream of nitrogen. Never the powder was put in contact with pure ammonium perchlorate and a well defined sequence of the reagents in the propellant preparation was established to avoid this event. Each powder sample was tested before the preparation in very small weight to investigate the reactivity and the safety degree. The operator was equipped with gloves, goggles and an antistatic device. Small quantities of the metal which are not recyclable or recovered are destroyed by treatment with a dilute solution of hydrochloric acid.

Friction, impact, moderate temperature increase, etc. do not hinder laboratory handling of nano-Al. Electrostatic discharges may be risky and thus require proper attention. Mix of 100 g are routinely manufactured and handled at the SPLab with the precautions usually taken when highly energetic materials are employed.

5.2 Experimental Technique

Propellant samples (4.5 x 4.5 x 30 mm) of the formulations under examination were burned in a nitrogen-flushed window bomb in order to measure the steady burning rate. Samples were ignited by a hot Nichrome wire. Pressure was kept constant during the whole combustion process with a feedback pressure control system. Steady burning rates were measured in the range 1-70 bar, using an automated image processing technique from high-speed video recordings. Several samples (at least 3) were used for each experimental point and for each sample several burning rate readings were performed, according to well-established SPLab procedures.

5.3 Comparative Results

5.3.1 Micrometric vs. Nanometric Al powder: Partial or Full Replacement (AP-2)

As shown in Fig. 5.2 propellant P_06, assumed as baseline, has the lowest burning rate. All remaining formulations containing nano-particles exhibit significantly higher burning rates, thanks to the strong reactivity of the nano-sized Al particles[1-2]. By replacing 50 µm Al flakes with the same amount of 0.17 µm nano-Al, burning rate approximately increases by 40% (P_07_B02b), 60% (P_08), 100% (P_02b) respectively corresponding to 20%, 50%, 100% nanometric replacement of the micrometric Al powder. Thus, steady burning rates increase by increasing the fraction of ultra-fine Al. For both monomodal Al distribution propellant (P_05) and bimodal Al distribution propellant (P-09), no significant burning rate difference is observed for 50 µm Al flakes replacing 30 µm Al spheres.

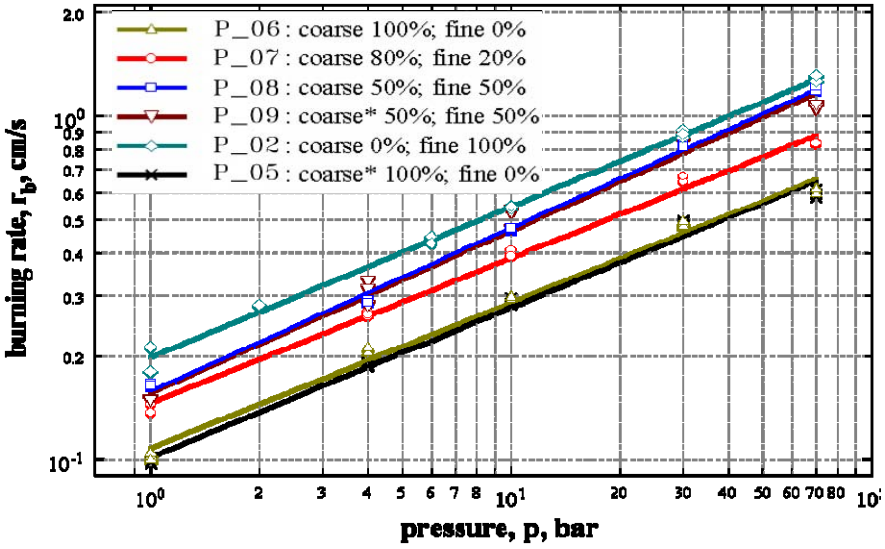

Fig. 5.2. Increasing steady burning rates with decreasing c/f fraction of Al powder (Series I propellants, bimodal AP-2).

5.3.2 Micrometric vs. Nanometric Al Powder: Size Effect (AP-2)

The second propellant series shows a similar trend, as illustrated in Fig. 5.3. Formulations including different nano-Al powders (type 04a and 01a of Table 1) feature significantly higher burning rates, while Al particles in the range 2.5 to 50 µm (type 03d, 05, and 06) makes no appreciable difference.

In AP-based composite propellants AP grains, after a crystalline phase transition (from orthorhombic to cubic at 513 K), undergo an exothermic degradation generating hot gases. Approximately, 70% of AP degrades through this exothermic reaction, while the remaining 30% sublimes into NH_3 and $HClO_4$, which then react in a premixed flame, very close to the burning surface, over a distance of about 0.5 µm (against 20 µm of the main diffusive flame) under normal rocket pressures. Combustion gases, characterized by a rich oxygen content, mix with hydrocarbon gases generated by the pyrolyzing binder and react in the main diffusion flame responsible for the conductive heat flux to the burning surface, which supports the degradation of both AP and binder.

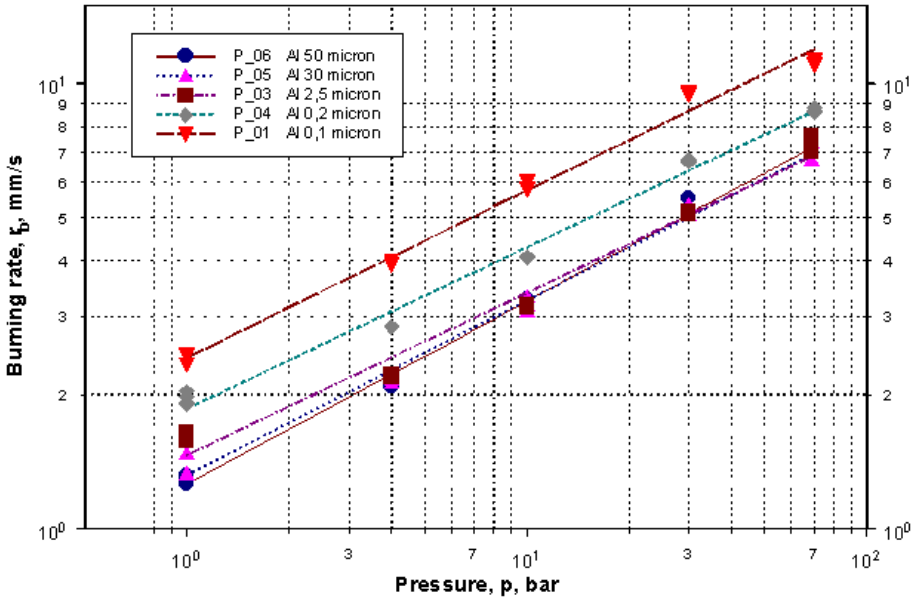

Fig. 5.3. Increasing steady burning rates for decreasing Al powder size (Series II propellants, bimodal AP-2).

Metal powders in the micrometric range (or above) burn according to a distributed mechanism extending much beyond the gas-phase flame thickness and thus not affecting the essentially diffusive combustion process just described. However, experimental results in the nanometric range show a remarkable steady burning rate augmentation with either increasing replacement of micrometric by nanometric Al (Fig. 5.2) or decreasing size of the nanometric Al (Fig. 5.3). The fact that ultrafine metal particles neatly increase steady burning rates testifies that the gas-phase flame structure is now affected by the combined effects of possible earlier ignition and quick premixed burning. The fact that the burning rate increase is further enhanced by decreasing size of nanometric Al points out a primary effect of specific surface, typically increasing by at least an order of magnitude from micrometric to nanometric Al.

Within the explored operating conditions of Figs. 5.2-5.3, the basic flame structure appears only slightly affected, as revealed by the minor changes of the burning rate pressure sensitivity. In agreement with other studies, the findings can be summarized as follows:

- for bimodal Al formulations, replacing micro with nano Al yields a neat increase of burning rates with growing fraction of nano Al;
- for monomodal Al formulations, decreasing nano Al size yields a prominent increase of burning rates in the range 0.1 - 0.2 μm.

5.4 Effect of Nano-Al Nature

5.4.1 Nanometric Al powder type 01

The most remarkable ballistic effects among all nano-Al so far tested were given by nano-Al type 01a (nominal size 100 nm, measured actual size somewhat larger). A detailed physical characterization revealed a bimodal distribution of the powders with bigger particles in the range 200-300 nm scattered in a significant fraction of nano-particles of spherical shape in the range 10-50 nm.

Nano-Al type 01b and 01c were received only recently and tests are currently in progress.

5.4.2 Nanometric Al powder type 02: effects of age on burning rate

The steady burning rates of three identical formulations differing only for the time production of the used nano-Al type 02 are reported in Fig. 5.4. The formulations using nano-Al of recent production (2a and 2b) showed very close results, while the formulation using nano-Al of old production (2c) featured a moderate but systematic increase of burning rate.

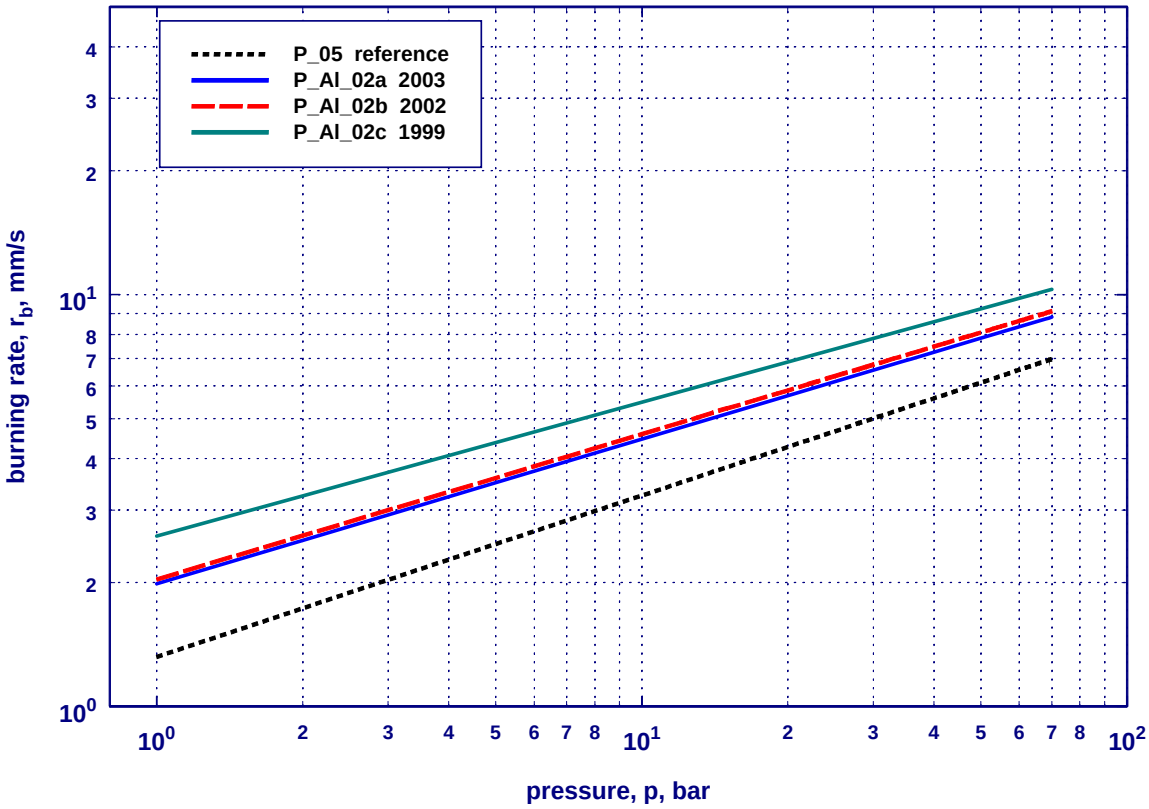

Fig. 5.4. Increasing steady burning rates with ageing of bimodal Al type 02 (bimodal AP-1).

The physical characterization of the powders so far attempted failed to reveal any significant differences among them: the crystalline metallic Al decreases from 95.5% to 92.2% while the crystalline AlN increased from 4.3% to 7.8%. However, a literature survey shows that ageing of Al particles may be important. In fact:

- no significant effects take place for 17 µm (or more) Al particles, protected by a natural oxide layer of 0.5 µm thickness;
- on the contrary, important effects take place for EEW nano-Al in the range 0.1- 0.2 µm, due to surface deterioration leading to $Al(OH)_3$ formation rather than Al_2O_3 and adsorption of gas (2-7% against 2-5% of oxidation products and 86-92% of Al metal for Alex);
- in general, anti-ageing coatings need to be implemented for passivation: for example, the commercial L-Alex uses an organic coating of palmitic acid.

5.4.3 Nanometric Al powders type 03: a peculiar behavior

An effort was made to discriminate burning rates in the range 0.2 – 2.5 µm using nano-Al type 03. For propellants P_03-a and P_03-b, containing the same kind of Al type 03, the only difference is the nominal particle size, respectively 0.2 µm and 0.4 µm.

Although showing an increased burning rate and decreased pressure exponent with respect to micro-Al (see P_06 and P_05), the two obtained rate curves are very close (Fig. 5.5). In fact, SEM analyses indicate that the real dimension of both Al powders is centered around 1.7 µm, with some minor differences in their size distributions around the average value, explaining the overlapping of the burning rate curves. The actual distribution of the Al powder type 03b and type 03c shows respectively a characteristic size of 1.73 µm and 1.86 µm, revealing rather a micrometric dimension of the corresponding Al grain sizes. Similar results were found for the Al powder type 03a. For all nano-Al type 03, the only recognized crystalline phase is metallic Al with no AlN. Also, the typical properties of nano-structures well manifest in nano-Al type 01a are missing in type 03. This surprising result stresses the need of a full characterization of the used nano-Al independently on their nominal specifications.

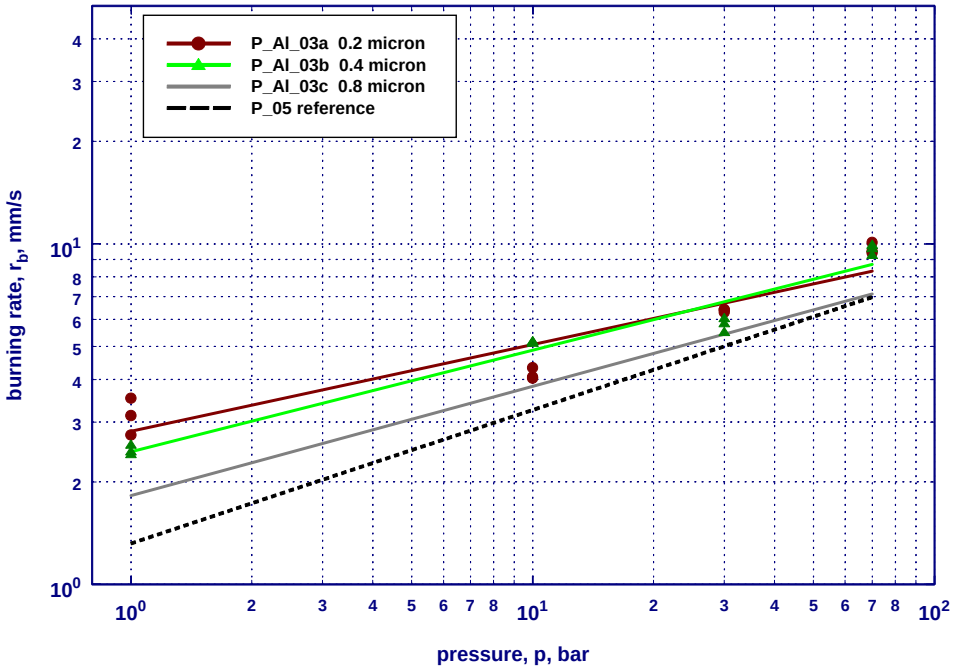

Fig. 5.5. Similar steady burning rates for bimodal Al type 03a and 03b (bimodal AP-1).

5.5 Summary of experimental steady burning rate laws

The standard Vieille ballistic laws and densities measured for the indicated tested compositions are summarized in Table 5.5. A common remark is that monomodal nano-Al formulations (P_01a, P_02b, and P_04a) yield higher propellant densities than micro-Al formulations (P_06 and P_05).

In Series I propellants, bimodal Al compositions (P_07_B, P_08, P_09) with bimodal AP-2 and HTPB R-20 binder feature, with respect to the baselines P_05 and P_06, a burning rate sensibly increased by nano-Al replacement while the pressure sensitivity trend is slightly increased (manual mixing).

In Series II propellants, monomodal Al compositions (P_05, P_04a, P_03d, P_02b, P_01a) with bimodal AP-2 and HTPB R-20 binder feature, with respect to the baselines P_05 and P_06, a burning rate sensibly increased by decreasing monomodal nano-Al (P_04a, P_01a) while the pressure sensitivity trend is slightly affected.

In Series III propellants, all with bimodal AP-1 and HTPB R-20 binder, with respect to the baselines P_05 and P_06, bimodal nano-Al type 02 (compositions P_Al _02a, P_Al _02b, P_Al _02c) yields increased burning rates while pressure sensitivity is slightly decreased. Likewise, bimodal nano-Al type 03 yields burning rates sensibly increased while pressure sensitivity is decreased; this effect is more marked for nano-Al type 03a and 03b (compositions P_Al _03a, P_Al _03b) and less for Al type 03c (composition P_Al _03c). About the same effect is observed for bimodal nano-Al type 04a and 04b (compositions P_Al_04a, P_Al_04b). The reason being the fact that all of these propellants have the same formulations except for a

20% replacement of 30 µm Al with the same amount of the corresponding nano-Al, notwithstanding the different production technique (EEW for nano-Al type 02 and type 03 but plasma condensation for nano-Al type 04).

Minor discrepancies are possible in the summarizing Table 5.5 due to the large number of experimenters and prolonged time span of experimentation.

Table 5.5 - Best fitting of Vieille steady burning rate law for tested propellants.
(in progress)

Propellant Short Notation	Density, g/cm^3	Vieille burning rate law, $r_b = a\ p^n$	
		a, mm/s	n, (mm/s)/(bar^n)
P_01a	1.67	2.42 ± 0.07	0.38 ± 0.01
P_02b	1.67	2.00 ± 0.04	0.44 ± 0.01
P_03d	1.56	1.46 ± 0.06	0.37 ± 0.01
P_04a	1.69	1.86 ± 0.04	0.36 ± 0.01
P_05	1.52	1.32 ± 0.03	0.39 ± 0.01
P_06	1.59	1.08 ± 0.03	0.42 ± 0.01
P_07-B01	1.63	2.04 ± 0.07	0.35 ± 0.01
P_07-B02b	1.60	1.47 ± 0.03	0.42 ± 0.01
P_07-B03d	1.57	1.27 ± 0.10	0.44 ± 0.03
P_08	1.63	1.58 ± 0.03	0.48 ± 0.01
P_09	1.67	1.57 ± 0.07	0.47 ± 0.02
P_BL_05	1.56	1.89 ± 0.07	0.34 ± 0.01
P_BL_01	NAv	NAv	NAv
P_BL_02	1.63	3.25 ± 0.11	0.24 ± 0.01
P_BL_01a	1.65	5.17 ± 0.16	0.20 ± 0.01
P_BL_02a	1.61	3.53 ± 0.13	0.24 ± 0.01
P_Al_01a	1.61	2.61 ± 0.20	0.28 ± 0.03
P_Al_02a	1.61	1.99 ± 0.11	0.35 ± 0.02
P_Al_02b	1.61	2.04 ± 0.07	0.35 ± 0.01
P_Al_02c	1.53	2.59 ± 0.09	0.33 ± 0.01
P_Al_03a	1.52	2.82 ± 0.25	0.26 ± 0.03
P_Al_03b	1.56	2.45 ± 0.14	0.30 ± 0.02
P_Al_03c	1.58	1.82 ± 0.11	0.32 ± 0.02
P_Al_03d	NAv	NAv	NAv
P-Al_04a	1.65	2.11 ± 0.09	0.30 ± 0.02
P_Al_04b	1.64	2.93 ± 0.20	0.23 ± 0.02

6. RADIANT IGNITION DELAY

While ignition of solid propellants is a largely investigated subject[3-4-5-6], the behavior of compositions including ultra-fine powders is scarcely investigated. The ignition delay vs. radiant flux, from a continuous wave CO_2 laser source, was measured for several of the propellants investigated in this research project. The baseline propellant (P_05) showed the highest ignition delay. The reason can be attributed to the Al large thermal conductivity which slows down the surface temperature rise. By progressively replacing micro-Al with nano-Al, while keeping constant the total Al mass fraction (15 % for all the propellants considered), the ignition delay decreases. During laser heating, the enhanced reactivity of nano-Al powders manifests as an earlier build-up of the transient flame (leading to self-sustained combustion regime) with respect to not only micrometric Al but even unmetallized compositions. This is in qualitative agreement with the reported possible lower melting temperature of nano-Al[7] and quicker[8-9] ignition of nano-Al based reactive mixtures. Similar results were obtained under go/no-go and continuous radiation testing. But a perceivable data scattering is observed due to strong heterogeneity of the samples; in this respect, the flame appearance definition is influential. Slope of all ignition boundaries are much larger than the theoretical limit of -2 expected for opaque nonreactive propellants. For a matter of space, detailed results are not reported; a more complete discussion will be included in next report.

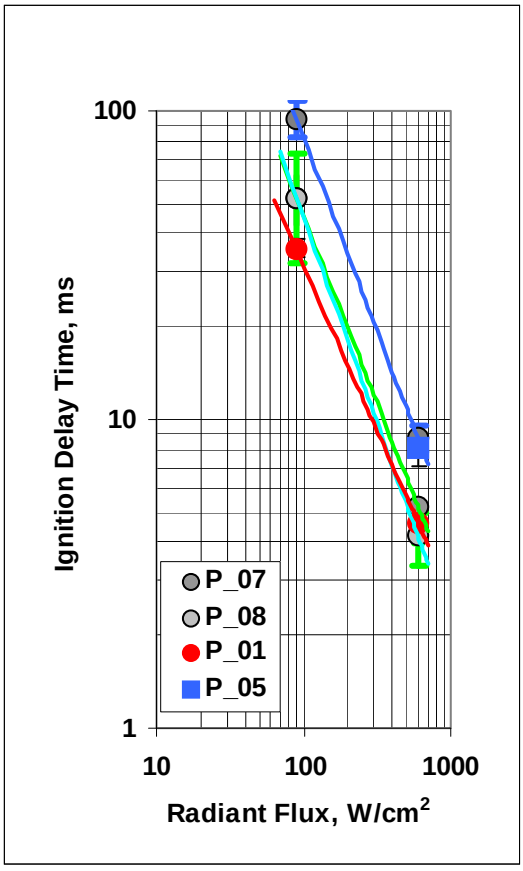

Fig. 6.1. Radiant ignition delay at 1 bar.

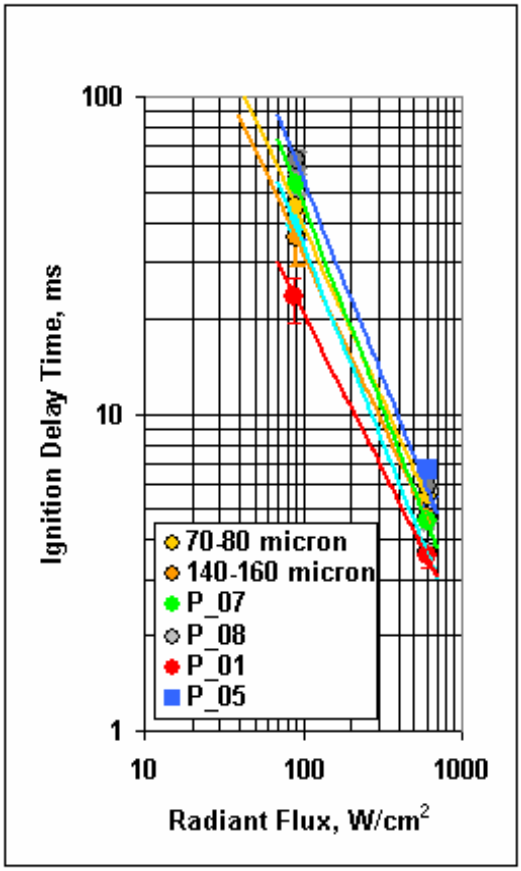

Fig. 6.2. Radiant ignition delay at 10 bar.

7. FLAME VISUALIZATION

7.1 Experimental

Visualization of combustion processes taking place in solid propellant burning was obtained by high-speed digital color video-camera. An effort was made to acquire pictures showing the complex details of the burning surface evolution and the interactions among the main propellant ingredients, a point of the greatest interest in all composite formulation. All theoretical models trying to describe/predict combustion rates as well as agglomeration phenomena (of paramount importance for metallized propellants) are based on severe assumptions about the nature and morphology of the combustion surface; a technique that is able to verify and/or offer guidelines about these assumptions is certainly useful.

In the past optical techniques could not be efficiently used because of the complexity, weight, and cost of cinematographic apparatus. Long times and a lot of patience were required both for careful optimization of the experimental setup and (slow) development of movies; at any rate the final result was not in the proper format for computer assisted processing. Digital video-cameras, in particular those resorting to the last generation of optical sensors, strongly alleviate most of the above problems and offer the possibility of real-time visualizations of complex combustion phenomena. This is particularly important when dealing with innovative propellant formulations.

Images were taken with a commercial high-speed digital color camera with the following operating features:

- **Sensor:** CMOS (Bayer system color, single sensor) with 17µm pixel, 4µs global electronic shutter and overexposure protection.
- **Shutter:** Global electronic shutter from 10ms to 4µs.
- **Frame Rate:** Up to 120,000 fps.
- **Resolution:** Up to 1024x1024 depending on frame rate (full resolution up to 2000 fps.
- **Lens Mount:** "C" mount 12x Zoom Navitar.
- **Internal Memory:** 8 Gbytes of RAM memory.
- **Dimensions and Weight:**
  Camera Head: (no lens mount) 4.72" (120 mm) H x 4.33"(110 mm) W x 3.34" (92.2 mm) D
  Weight: 2.2 lb (1 kg) DC.
  Processor: 8.39" (213.1 mm) H x 5.51" (140 mm) W x 12.08"(306.8 mm) D
  Weight: 12.13 lb (5.5 kg) DC, 18.74 lb (8.5 kg) AC.

The implemented optical system is characterized by a resolution, in terms of lens system's ability to image closely spaced points, lines and object surfaces as separate entities, of 11.90 µm under the minimum magnification conditions (x 0.87) and 2.22 µm under the maximum (10.50). However, the optical sensor connected with the lens system features a resolution of 39.08 – 3.24 µm with the same magnification: thus, the system is "camera limited".

Several visualizations were effected of a variety of metallized composite formulations:

- a commercial AP-based propellant, metallized with 18% of propulsive Aluminum type 05;
- AN–based propellants, metallized with 15% of commercial Aluminum type 06;
- AP–based propellants, metallized with 15% of different kinds of nano–Aluminum;
- AP–based propellants, metallized with various amounts of AlH_3.

	Metal	Oxidizer	Binder
AP micro-Al	18% type 05 Al	68% AP	14% HTPB
AN	15% type 06 Al	68% AN	17% HTPB
AP nano-Al	15% nano–Aluminum	68% AP	17% HTPB

7.2 Aluminized Composite Propellants

7.2.1 Burning Mechanism by Visual Inspection

High-speed optical observations by digital video-cameras conveniently illustrate the propellant burning surface regression accompanied by binder decomposition and oxidizer particle combustion (under the tested operating conditions, the occurrence of a liquid layer is manifest for AN but not for AP crystals). The columnar nature of the convective hot gas flow, issued by the heterogeneous burning surface, is also well discernible.

The combustion of aluminum fuel is nonetheless the process of vital interest in this study[10-11-12-13-14]. The Al powder is initially located among the coarse fraction of the oxidizer particles (in areas often called pockets) and also, if $d_{AP}/d_{Al} >>1$, in the narrow channels of interpockets connections (in areas often called bridges). In both areas, Al powder is immersed in the intermediate decomposition products of the binder and possibly of the fine fraction of the oxidizer particles as well (making the resulting propellant microstructure in general very fuel-rich). The traveling deflagration wave starts the propellant combustion process by conductive and maybe radiative heating of the fresh composition material. Once it reaches its melting point of 933 K, Al becomes liquid but is still isolated by a protective hard and refractory oxide shell from the surrounding hot and oxidizing reactive atmosphere. The low volatility of Al (with a boiling temperature about three times larger than the typical propellant surface temperatures) and its intimate mixing mainly with the combustible binder are additional factors conspiring against Al powder ignition. However, the Al particles, covered by the external hard oxide shell, during heating undergo a process of rupture/crack of the shell due to the larger thermal expansions coefficients of the metal wrt the oxide and a 6% volume increase upon metal melting. These physical effects make possible for liquid Al to flow freely exposed to the surrounding chemically and thermally excited atmosphere, thus triggering Al ignition and combustion in general by evaporation sustained diffusion. For nano-Al, a premixed rather than diffusion flame is likely to take place. At any rate, heterogeneous combustion is also possible.

Cracking of the protective hard oxide shell actually involves a variety of additional effects[15] affecting in a multifaceted way the already intricate heating - ignition - combustion events. When the temperature is below the Al_2O_3 melting point of 2345 K, liquid Al leaking through a single or multiple ruptures of the external hard oxide shell is subjected to oxidation thus promoting resealing of the fractured shell. This mechanism also offers a possible way for the solid metal particles, initially separated, to physically join in complex clusters by sintering. For nano-Al, resealing is less likely to take place and thus easier ignition may be promoted[16-17-18]. See pictures in Fig. 7.7. Further sintering effects may occur directly in the hot portion of the thermal wave near the burning surface layer.

Visual inspections performed during this investigation reveal for AP/hydrocarbon binder formulations a common fundamental burning mechanism. This is based on the exudation, emerging over the combustion surface from the propellant microstructure, of solid aggregates of aluminized nature and different structure; see images in Fig. 7.1 (micro-Al) and Fig. 7.2 (nano-Al). These aggregates exude from the propellant, grow on the burning surface, accumulate, and protrude in the adjacent gas-phase until detach due to exhausting (no more anchorage below the surface) or a variety of external effects; see magnified image in Fig. 7.3. Prominent detachment reasons experimentally observed are:

1. full / partial combustion near the burning surface. This mechanism of fast disappearance by chemical consumption is apt to lessen incomplete burning and specific impulse losses.
2. Inflammation[19] (progressive & self-accelerated ignition of, and flame propagation over, the accumulated exudation aggregates), started by the surrounding hot gas and sustained by the subsequent combustion heat release. Inflammation ultimately leads to coalescence by meltdown of the whole exudation material into a large burning agglomerate, triggering a sort of chemical implosion effect. The geometrical shape undergoes an amazing metamorphosis from widely different complex solid structures to a very regular spherical droplet due to the high surface tension of liquid Al; see magnified image in Fig. 7.4. The liquid Al_2O_3, being insoluble in liquid Al, retracts into lobes/caps; in addition, solid Al_2O_3 may also be randomly trapped inside the droplet. Burning reduces the droplet surface tension and causes hot combustion gases to expand, thus promoting the droplet lift off. This mechanism of slow disappearance by chemical consumption is a probable cause of incomplete burning and the main responsible of specific impulse losses.
3. Downstream entrainment and some kind of degradation by the surrounding hot gas flow. This mechanism of fluid dynamic entrainment moves far downstream the accumulated exudation aggregates and the related degradation process. It probably contributes to incomplete burning and to specific impulse losses as well. The actual fate of the entrained material depends on the specific

operating conditions. In the experimental apparatus used in this investigation, the entrained aggregate escapes out of the view field; see image in Fig. 7.10

On the other hand, exuded aggregates and/or incipient burning agglomerates, tending to leave the combustion surface due to the surrounding convective flow entrainment and hot gas expansion caused by burning, are stuck by retention forces associated with the:

1. viscous molten binder not yet fully gasified (main effect) and maybe other molten material;
2. carbonaceous surface layer structures (well evidenced for AN oxidizer, where the loaded metal particles form drops scattered all over and filling the porous carbonaceous surface layer grid allowing the initially solid metal particles to physically join); see Babuk[20-21-22-23-24];
3. direct adhesion (sintering) to underlying Al particles (see Price[19]);
4. possible acceleration effects (see Bandera 2004).

7.2.2 AP based micro-Al propellants

High-speed video-recording shows agglomerates of often perfectly spherical shape made by an opaque mixture (solid + liquid) of retracted Al_2O_3 lobe / cap contrasting the gas-phase combustion of the luminous molten Al droplet above (in the convective flow direction). See images in Fig. 7.1 (transition from exudation to agglomerate), Fig. 7.4 (magnification of a spherical agglomerate), and Fig. 7.5 (overall view of emerging exudation and successive agglomeration at some distance from the surface). Similar phenomena are observed for flaked micro-Al type 06; see images in Fig. 7.8.

Aluminum particles or agglomerates commonly burn somewhat far from the surface in both heterogeneous and gas phase homogeneous mode; aluminum particles may also burn near the surface in both heterogeneous and gas phase homogeneous mode. The typical agglomerate burning is characterized by the presence of an oxide cap and by the gasification of aluminum: a flame is visible around the spherical agglomerate with the formation of the so called “SOP” (small oxide particles) that follows the convective hot gases flow. Unburned particles probably containing aluminum, aluminum oxide, and intermediate binder decomposition products are also visible in the convective flow. The droplet temperature is estimated around 2500 K (above the Al_2O_3 melting point of 2345 K and below the Al boiling point of 2740 K at 1 atm) with peaks up to 3800 K in the heterogeneous part of the flame; see Price[10-11-19] for details.

7.2.3 AP based nano-Al propellants

Compared to micrometric size Al, nano–Al combustion near the burning surface results to be much more luminous with exudation of thin flakes of coralline structure from the propellant microstructure. Again, these solid aggregates exude, grow on the burning surface, accumulate, and protrude in the adjacent gas-phase until exhausting. See images in Fig. 7.2 (emerging exudation flakes), Fig. 7.3 (magnification of a coralline flake), Fig. 7.6 (reduced agglomeration under the tested operating conditions), and Fig. 7.9 (overall view showing profuse exudation flakes and frequent near surface transition to agglomerates). Forced detachment may occur earlier due to:

1. quick combustion near the burning surface (high reactivity of nano-Al size);
2. easy inflammation by the surrounding hot gas and quick coalescence into comparatively smaller agglomerates of spherical geometry (high reactivity of nano-size Al)
3. downstream entrainment and some kind of degradation by the fast gaseous flow issuing from the burning surface (high burning rate).

Because of the high reactivity of nano-Al (owing to large specific surface, low probability of resealing, etc.), substantial Al combustion likely takes place within the narrow and very luminous layer adjacent to the burning surface. The temperature increase is testified by the incandescence of the flakes and/or particles (see also Weiser et al.[25]). Single particles are probably consumed by a premixed mechanism, rather than diffusive, very near the surface and unlikely go anywhere far downstream. On the other hand, the short residence time hinders the accumulation of aggregates and its coalescence by inflammation into the large spherical agglomerates commonly observed for micro-Al; see image in Fig. 7.6. However, for the fraction of aggregates coalescing into agglomerates, the fate is just the same described for micro-Al.

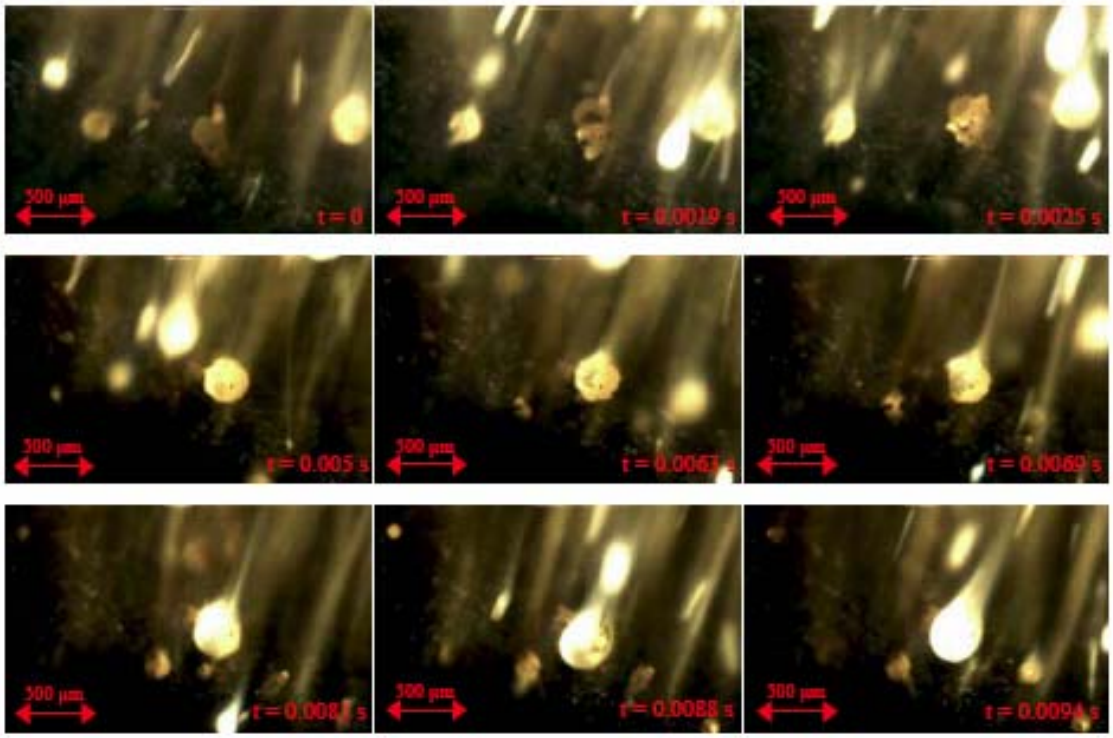

Fig. 7.1. AP based micro-Al propellant showing metamorphosis from exudation aggregates to spherical agglomerates (see central part of each frame). 8000 fps; digital shutter 1/8000; magnification 3x.

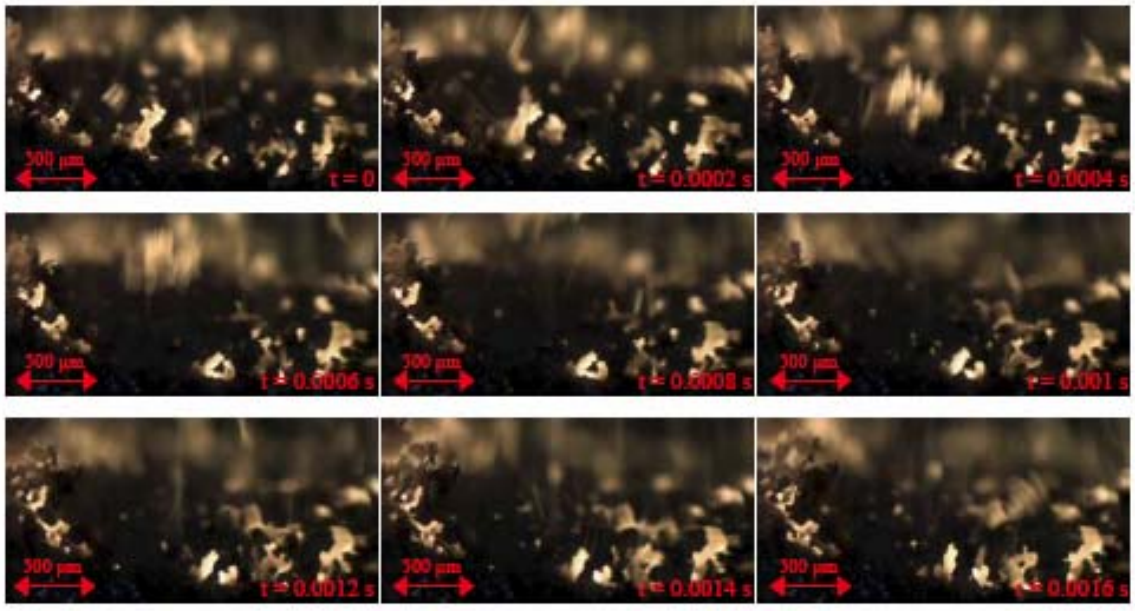

Fig. 7.2. AP based nano-Al propellant showing thin coralline exudation flakes emerging from the propellant microstructure. 10000 fps; digital shutter 1/10000; magnification 3.75x.

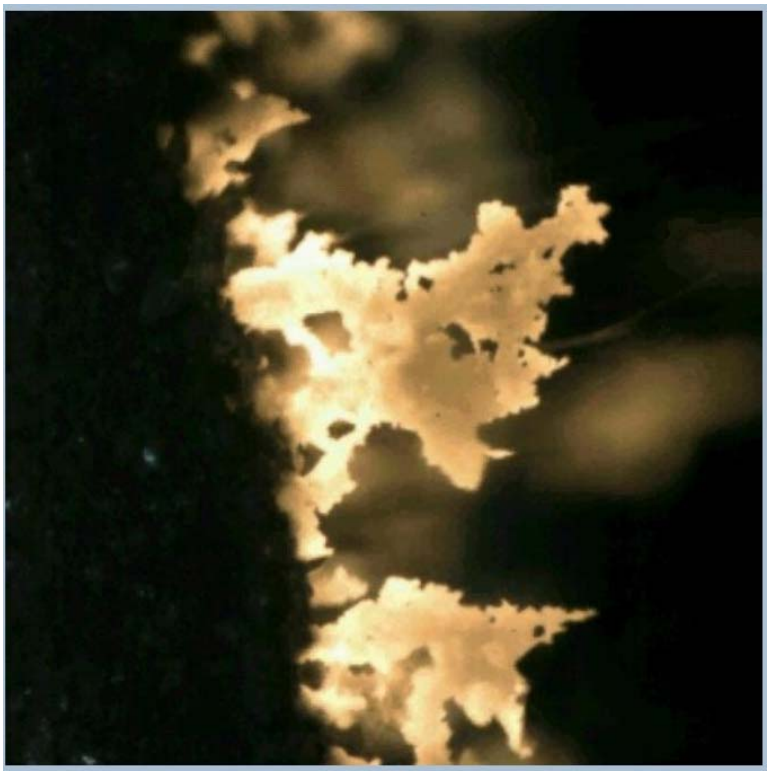

Fig. 7.3. AP based nano-Al propellant: magnified view of the exudation emerging from the propellant microstructure as aluminized thin flakes of coralline structure (pre-agglomeration stage).

Fig. 7.4 - AP based micro-Al propellant: magnified view of a spherical agglomerate following inflammation of the aluminized exudation aggregate from the propellant microstructure.

Fig. 7.5. 30 μm spherical micro-Al in AP/ HTPB, burning at 10 bar, showing exudation aggregates over the surface and agglomeration after inflammation at some distance from the surface.

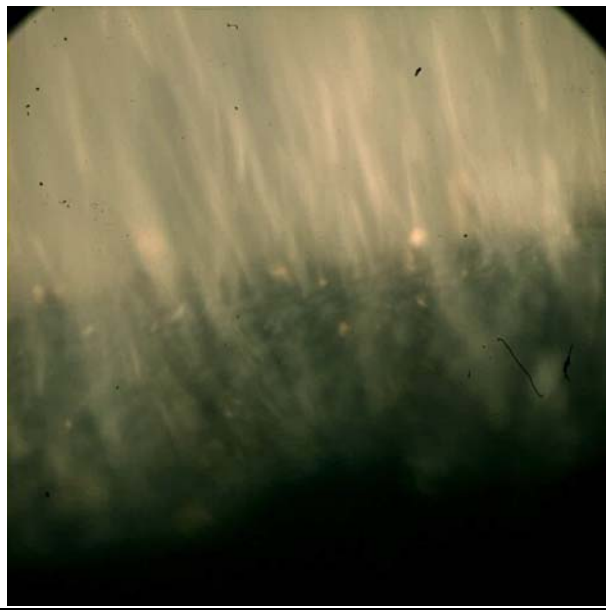

Fig. 7.6. 0.1 μm nano-Al in AP/PPG, burning at 10 bar, showing exudation aggregates over the surface and radically reduced agglomeration

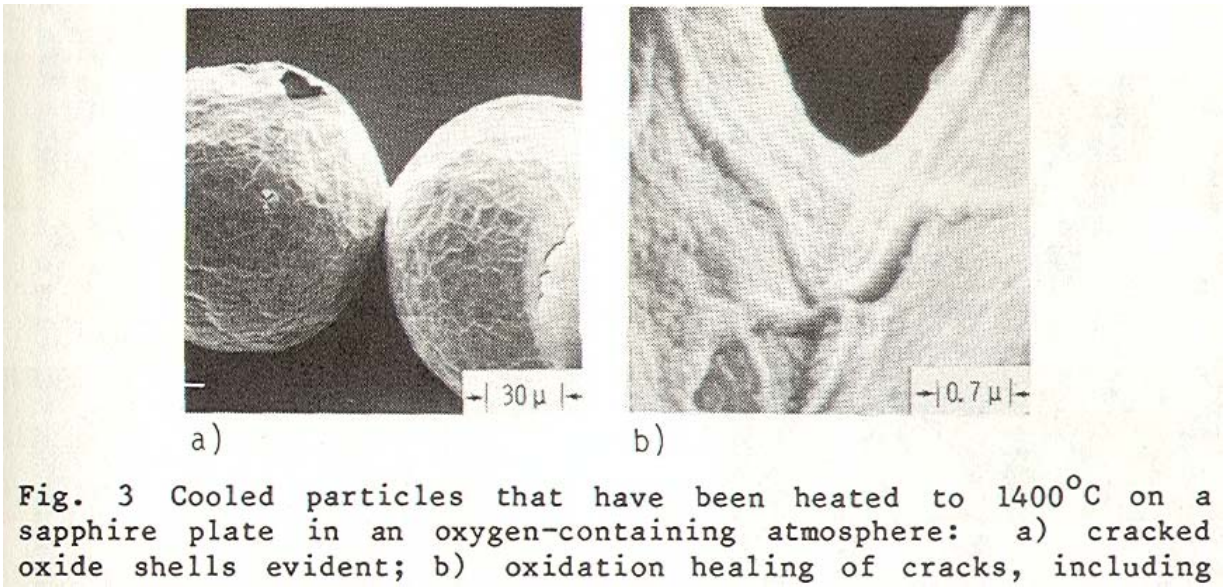

Fig. 3 Cooled particles that have been heated to 1400°C on a sapphire plate in an oxygen-containing atmosphere: a) cracked oxide shells evident; b) oxidation healing of cracks, including

Fig. 7.7. Ruptured external oxide shell (a) and magnified view of the contact point following inter-particle oxidation resealing (b); pictures taken from Price[11 above].

7.3 Unifying Concepts

The aluminized aggregate mass evolve in time subjected to a variety of forces in a chemically, thermally, fluid dynamically active environment and thus may effectively forget the features of the initial propellant formulation. The agglomerate size (central for propulsive performance) depends on the size reached by the aluminized aggregate mass just prior to inflammation. Circumstances conducive to large amount of aluminized aggregate accumulation near the burning surface favor the formation of large spherical agglomerates. These circumstances mainly refer to propellant formulation and burning rate:

1. large amount of aluminum in the oxidizer coarse fraction inter-particle pockets and maybe bridges;
2. binder of high thermal stability and high viscosity of intermediate decomposition products;
3. large residence times of the aluminized aggregates, possibly affected by steady or random inertial forces.

The propellant formulation in terms of nature, ratio, size of the ingredients (when applicable), and especially the detailed random packing of the solid fraction tend to control the accumulation of the exuded aggregate mass. Cold (i.e., pre-burning) aggregation of Al particles may take place before and during propellant manufacturing. This effect of exudation – accumulation repeats in time with a period of the order about of the coarse oxidizer particle burning time[10].

Large residence times favor the further accumulation of aggregates, inflammation, and coalescence into large spherical agglomerates close to the burning surface. This happens for:

1. slow or no combustion in the hot gaseous layer near the burning surface (low Al reactivity);
2. delayed inflammation (for example, resistance to ignition of aggregates due to high runaway temperature);
3. low burning rates due to propellant formulation in terms of nature, ratio, size of the ingredients (when applicable), and possible presence of burning rate modifiers; adverse operating conditions such as low pressure and/or low initial temperature; possible presence of a thick molten layer and its viscosity; etc.
4. Even for identical formulations, the specific experimental setup may discriminate the exudation – accumulation - inflammation - agglomeration – combustion train of events, in that vertical downward burning configuration favors the whole train of events while horizontal or vertical downward burning configurations hinder agglomeration.

The residence time is inversely proportional to the average propellant burning rate, possibly affected by steady or random inertial forces.

For large residence times, the continuous action of the retention forces overcoming the driving force (convective flow entrainment and hot gas expansion caused by burning) allow not only surface layer exudation to accumulate but also – under particular conditions - agglomerates to grow up and move somewhat on the surface. This situation is found in AN formulations and may lead to very large burning particles of the order up to 1000 µm. Just the opposite was observed for AP formulations containing AlH_3 instead of Al, owing to small residence times associated with large burning rates.

Data collection over a range of operating conditions (pressure, binder, Al size, etc.) points out that:

1. depending on the experimental details, combustion of agglomerates may start and complete either near the burning surface or far downstream; typically, inflammation occurs near the burning surface and combustion completes more or less far downstream.
2. Inefficient downstream entrainment and degradation (slow convective flow velocity) favors accumulation, while quick downstream entrainment (large convective flow velocity) avoids accumulation but it should be accompanied by fast degradation to avoid possible far downstream agglomeration.
3. Although coalescence of the exuded aggregates into inflamed spherical agglomerates gradually decreases with decreasing micro-Al size in the range 90 - 15 µm, a sharp decrease of flame heterogeneity (number and speed of particles / agglomerates) is only observed for nano-Al in the range 0.2- 0.1 µm and below (see also Bui et al.[26]).
4. The overall train of events (aggregation in the propellant microstructure - exudation over the burning surface – accumulation and evolution above the burning surface - inflammation - agglomeration – combustion) is too complex and is subjected to too many variables to be amenable to a simple analysis and set of results.
5. The same fundamental mechanism, however complex, seems to govern AP or AN based composite propellants, containing micro or nano Al, metallic or hydride Al fuels.

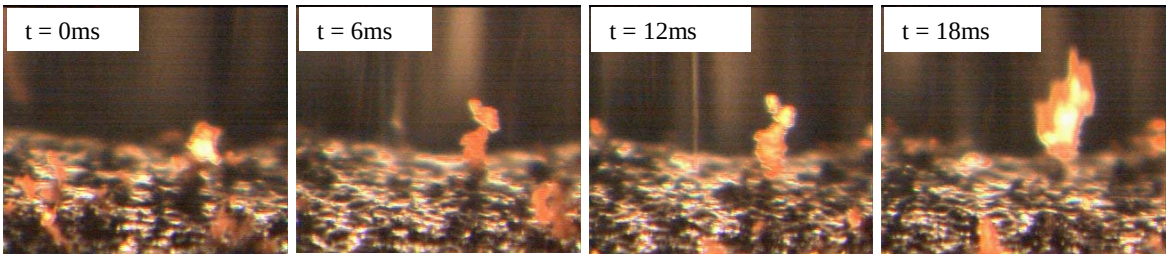

Fig. 7.8. Burning surface of 50 µm Al flakes formulation at 2 bar, showing some thick exudation aggregates over muddy burning surface and rare transition to agglomerates.
P_06 propellant, exposure time 1/500 s.

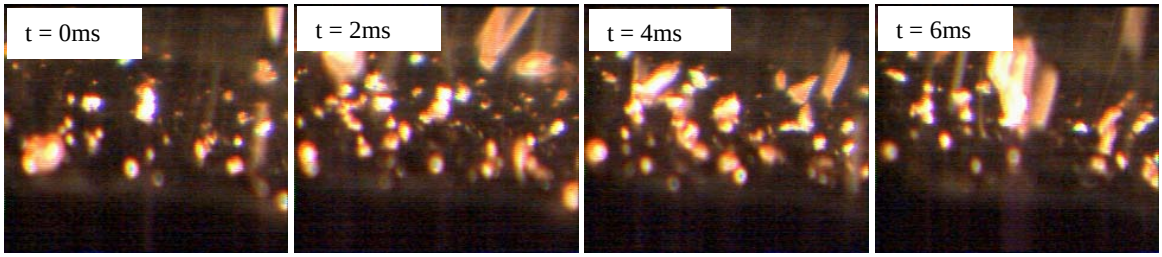

Fig. 7.9. Burning surface of 0.1 µm nano-Al formulation at 2 bar, showing profuse thin exudation aggregates over luminous burning surface and frequent transition to agglomerates.
P_02b propellant, exposure time 1/4000 s.

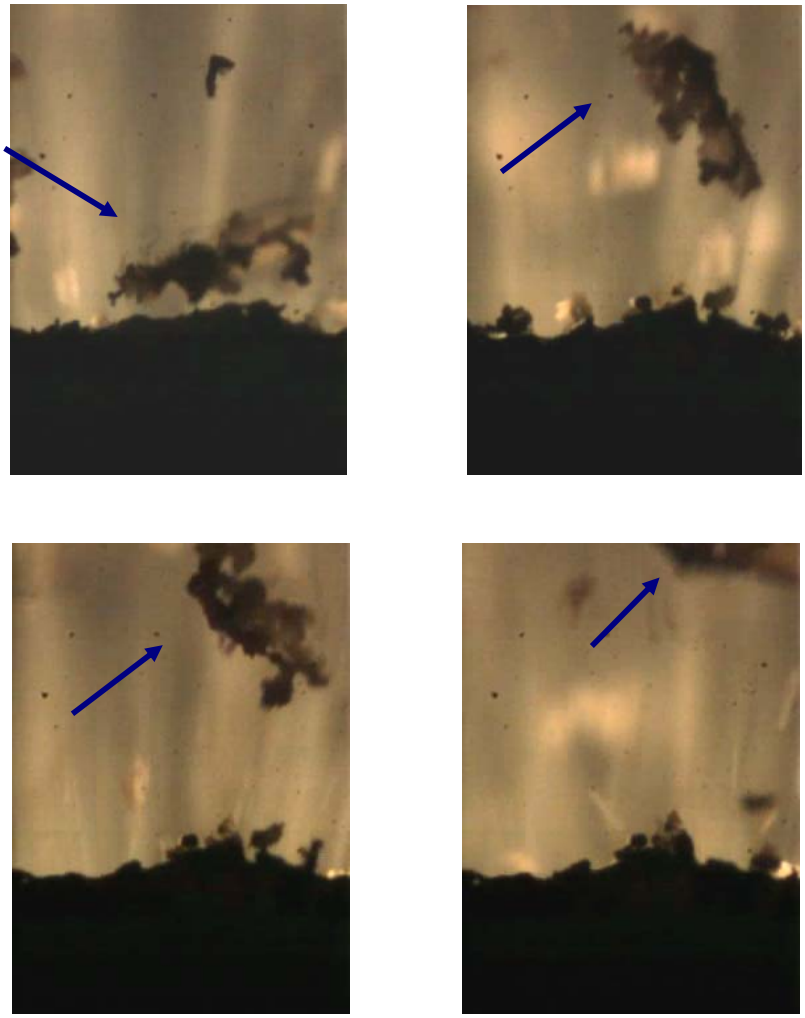

Fig. 7.10. AP based nano-Al propellant P_BL_01c at 10 bar showing exudation aggregates and entrainment of aluminized coralline flakes by the hot convective gas flow. 8000 fps; digital shutter 1/8000; magnification 2.5x; resolution 512x256.

Part IV POST BURNING ANALYSIS

8. RESIDUES ANALYSIS

8.1 Particle collection tests

The investigation of condensed combustion residues performed in this study aims to study the nano-Al powders influence on condensed products mass and oxidation development. A propellant sample (4.5 x 4.5 x 30 mm), mounted with the burning surface downward in a nitrogen-flushed bomb, is burned. After the propellant specimen combustion, the condensed combustion products are collected according to the technique later described. The collected products are then analyzed to determine their mass, their aluminum and aluminum oxide content, and a sample of them is analyzed in order to determine chemical composition and morphology. Experimental tests are performed at constant pressure of the combustion chamber. This is a definite strategy, considered the well known pressure influence on combustion residues. The automatic pressure control involves combustion products coming out from the chamber; they consist of gaseous products, also including a part of condensed products. Therefore it is evident that, at the present stage of the investigation, this approach bars the possibility to quantify the produced mass; but this limit does not contrast the aim of this work, devoted in this phase to investigate the influence of nano-Al powders on combustion products. As a consequence, the condensed products analysis performed and quantities shown in what follows, reveal trends which may represent a bearing for the future steps devoted to the investigation of the condensed combustion products based on separation of agglomerates and smoke oxide particles. In the following development of the work, therefore, the expression CCP means all condensed residues, including both agglomerates and smoke oxide particles.

The technique is based on the use of the experimental set-up shown in Fig. 8.1. The approach follows the procedure described by Babuk et al.[1], but in this case a pressure controlled vessel is used. The vessel walls are covered with a ice layer, 5 mm thick. The solution recovered at the end of the test is filtered in order to collect the condensed products. These are dried, and then treated with diluted hydrochloric acid, to dissolve the metal Al content of the residues and to estimate the Al oxide amount.

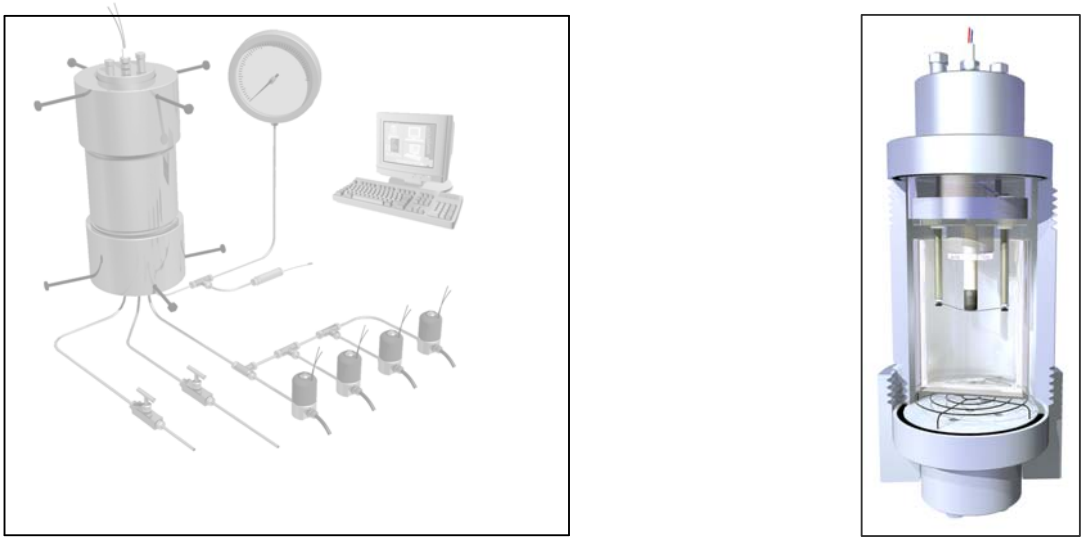

Fig. 8.1 – Experimental set-up used to collect CCP.

A special PES (PoliEtherSulphone) filter, designed for ultra-filtration and suitable for the treatment of acid solutions, characterized by a porosity of 100 KDa, proved to be the best choice. This porosity value allows to capture particles with a size larger than 5 nm. After the filter preparation, the solution is filtered, CCP are dried and the CCP mass is measured. Knowing that alumina is hydrochloric acid resistant, while Al is dissolved through the reaction:

$$2\ Al + 6\ HCl \rightarrow 3\ H_2 + 2\ Al\ Cl_3$$

which is rather fast at ambient temperature, the difference between the CCP original mass and CCP mass measured after the treatment with hydrochloric acid allows to determine the mass of unburned Al. Considering that the aluminum molecular mass is 26.98 g/mol and the alumina molecular mass is 101.96 g/mol, the measurement of these masses allows to define the following integral parameters:

$$\begin{cases} \zeta^{res}_{Al_2O_3} = \dfrac{2 \cdot 26{,}98}{101{,}96} \cdot \dfrac{M^{res}_{HCl}}{M^{Al}_0}; \\ \zeta^{res}_{Al} = \dfrac{M^{res} - M^{res}_{HCl}}{M^{Al}_0}; \\ \zeta^{res} = \zeta^{res}_{Al} + \zeta^{res}_{Al_2O_3}; \\ \eta^{res} = \dfrac{M^{res}_{HCl}}{M^{res}}. \end{cases}$$

The technique previously described was applied to a significant number of propellants. For propellants based on Al-powders of type 03 and type 04 only one propellant, representative of the family has been investigated.

A summary of results, obtained at a constant pressure of 30 bar, is presented in Tab. 8.1.

Table 8.1 - Experimental residue analysis for the indicated propellants at 30 bar of pressure.

	η^{res}	ζ^{res}	ζ^{res}_{Al}	$\zeta^{res}_{Al_2O_3}$
P_01	87.7	77.2	16.2	61.0
P_BL_02	85.7	67.7	16.2	51.5
P_05	84.2	65.2	17.0	48.1
P_Al_01a	87.1	71.6	15.7	55.9
P_Al_02a	89.4	58.4	10.7	47.7
P_Al_02b	91.4	59.8	9.1	50.7
P_Al_02c	91.0	63.0	9.9	53.0
P_Al_03c	80.9	68.5	21.1	47.4
P_Al_04b	78.0	76.7	26.7	50.0

Results of Tab. 8.1 confirm that nano-Al particles support a better oxidation.

Propellant P_Al_01a shows that, in terms of residues, the replacement of 20% of coarse Al particles with nano particles is enough to obtain the same characteristics of 100% nano-Al content.
Propellants of the Series _02 (a, b, c) show the highest fraction of oxides and the lowest fraction of unburnt aluminum in the residues. Ageing effects do not change significantly the behavior of the propellants manufactured with this powder.
Propellant P_Al_03c presents a fairly high content of unburnt aluminum and a corresponding low content of oxidized aluminum.
Propellant P_Al_04b has the highest content of unburnt aluminum in the residues (ζ^{res}_{Al}) and the lowest oxide fraction (η^{res}). The residues mass (ζ^{res}) is high but a significant fraction is made of unburnt metal.

8.2 SEM analysis

SEM allows a visual inspection of the combustion residues. SEM magnifications of combustion residues, collected at 1 bar and 30 bar chamber pressure, are shown in Fig. 8.1-8.4 for baseline propellants P_05 and P_01a. The micrographs are obtained by a SEM Cambridge Stereoscan 360, using an accelerating voltage of 20 kV and a working distance of 10 mm. SEM images of condensed combustion products, collected at 1 and 30 bar, highlight the shape of the agglomerates, shown for propellant P_05 respectively in Figs. 8.1 and 8.2. At the pressure of 1 bar the estimated average size of residues is 50 μm, while at 30 bar the average size is approximately 10 μm. The trend for P_01 propellant residues is not significantly affected by a pressure change as shown in Fig. 8.3 and 8.4; the average size is less than 10 μm in both cases. The general trend shown by SEM analysis confirms, for the investigated propellants and under the operating conditions used, that agglomeration is poor for coarse Al powder, but consistent for nano-Al powder. In the first case the nominal size of Al-powder contained in the propellant is 30 μm and the characteristic size of agglomerates is approximately 50 μm (increasing factor less than two), while in the second case the Al-powder size is 0.1 μm and the characteristic size of agglomerates is 10 μm, thus increasing by a factor of one hundred. This result, which points out a similar behavior of the condensed combustion products starting from differently sized Al-powders (30 and 0.1 μm), has to be considered together with the results of Tab. 8.2. The residues characteristic size is approximately the same but the Al oxide content (0.61 for P_01a vs. 0.48 for P_05), and the oxide content relative to the total residues mass (0.88 for P_01a vs. 0.84 for P_05) highlight the more efficient aluminum oxidation when nano-sized grains are used.

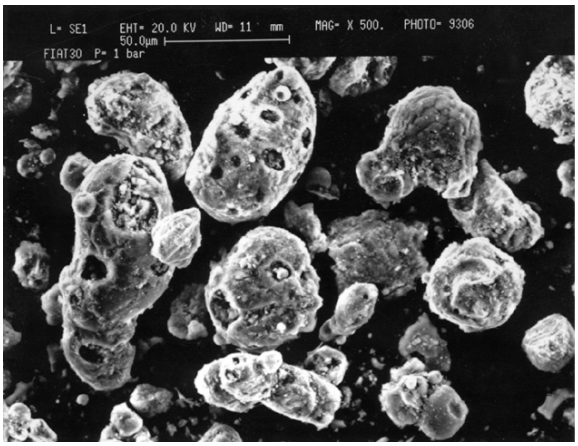

Fig. 8.1. SEM micrograph (x 500) of propellant P_05 condensed products at 1 bar.

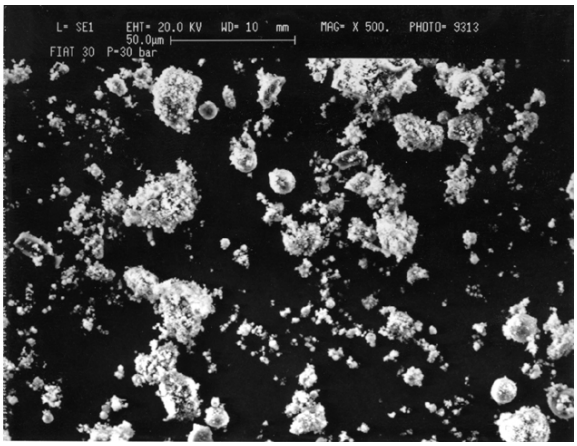

Fig. 8.2. SEM micrograph (x 500) of propellant P_05 condensed products at 30 bar.

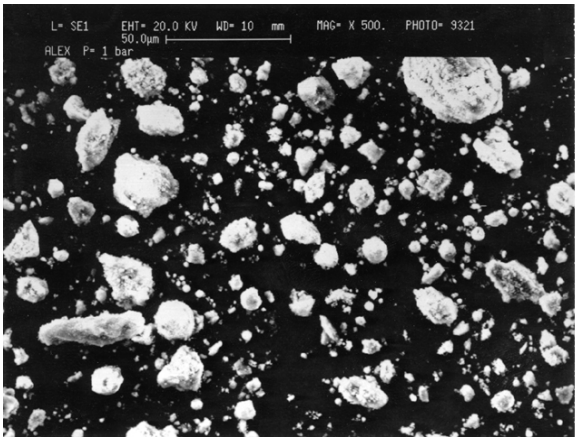

Fig. 8.3. SEM micrograph (x 500) of propellant P_01a condensed products at 1 bar.

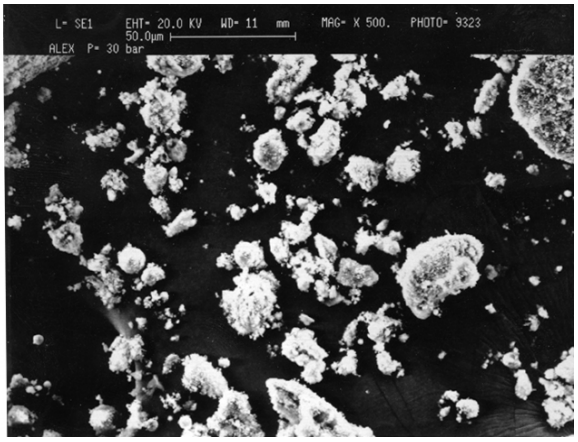

Fig. 8.4. SEM micrograph (x 500) of propellant P_01a condensed products at 30 bar.

8.3 XPS analysis

The XPS technique (X-ray Photoelectron Spectroscopy), also known as ESCA (Electron Spectroscopy for Chemical Analysis), is largely used to study the chemical composition of the surfaces. The spectrometer is a PHI-mod. 5500, with monochromatized aluminum source for X-ray production; spectra have been taken at 300 Watt. XPS was used to measure the chemical composition detected at the residues surface and to quantify the atomic concentration of chemical elements. Considering that XPS analysis concerns the surface of the residues, the bulk composition is better investigated by XRD. Further, XPS is a local analysis and the residue composition is known to be strongly heterogeneous; in spite of these characteristics, XPS allows to obtain interesting results: the detailed knowledge of the residue surface gives important information on the physico-chemical characteristics of the agglomerates, such as, for example, the carbon content and the nature of carbon bindings.

Tab. 8.2 shows the total amount of main atomic species in each state for the two baseline propellants P_01a and P_05.

Table 8.2 - XPS analysis of combustion residues (conc. at. %).

Propellant	Pressure (bar)	C1s	N1s	O1s	Al2s	Cl2p	Mg2p
P_ 05	1	17.4	0.2	46.8	30.2	2.4	2.5
P_ 05	30	16.3	0.4	45.7	36.2	1.3	---
P_01a	1	10.4	0.2	49.7	38.2	1.4	---
P_01a	30	19.4	0.2	45.1	34.0	1.1	---

A particular comment concerns the carbon content in the combustion products. In the propellant combustion processes the products obtained from the binder depend on the chemical composition of the binder itself. In particular the different carbon skeletons obtained influence the combustion processes of the metal. Binders made of unsaturated macromolecules, such as polyisoprene or polybutadiene (HTPB), at high combustion temperature tend to cure, thus giving origin to carbon structures, of graphitic type, fairly stable. Such a structure can host the aluminum particles for long enough to allow its combustion and its incorporation in aluminum oxide products. Binders made by saturated macromolecules, such as polyoxipropylene or polyoxiethylene, modified with isocianates, produce formation of less stable carbon structures which do not allow the metal to remain long on the carbon layer. Particles metal, in this case, burn quickly without agglomeration processes. It is known that polybutadiene, the binder used in this study, produces a large quantity of carbon residue. Therefore, carbon comes from pyrolysis processes and is partially oxidized. Al is the total Al, mainly detected as Al oxide, while metal Al contained inside CCP does not appear in the XPS analysis of the residues. Chlorine is probably chlorine from AP decomposition, entrapped in the CCP. Contamination metals, such as Sn, Cu, F, are eliminated after the HCl treatment.

8.4 XRD analysis

XRD spectra were collected step-wise using Cu K_α radiation (λ=1.5416 Å) on a computer controlled Philips X'Pert PRO $\theta/2\theta$ diffractometer, equipped with a secondary curved pyrolytic graphite monochromator, in the 5-125° 2θ angular range, with 0.02° steps and 15 s counting time.

XRD spectra have been obtained to disclose the crystalline phases and their relative abundance. A qualitative analysis has been carried out by means of the Hanawalt search method on the data set PDF-2 (Powder Diffraction File, ICDD) [2]. In addition, a full-profile fitting procedure, based on the Rietveld method, allowed to perform very accurate quantitative analysis and to get complete structural refinements of each identified phase. The relative structure of each single phase comes from the ICSD (Inorganic Chemical Structure) data base [3]. All the Rietveld refinements have been performed using the software package GSAS (Generalized Structure Analysis System) [4].

The results of the X-ray powder analysis relative to the combustion products of baseline propellants P_01a and P_05 are summarized in Tab. 8.3. From the compositional point of view, all the analyzed residues

contain the same inorganic phases, that is γ Al_2O_3, δ*Al_2O_3 , α Al_2O_3 and metallic aluminum. The first two phases are metastable transition aluminas and the third one is the well-known Corundum. The aluminum content of residues suggests that the higher pressure favors the metal burning and that the burning performance of propellant P_01a is much better than P_05 ones: the metal Aluminum content (Al°) is much lower for propellant P_01a and aluminas content is larger for P_01a (except δ*Al_2O_3 at 30 bar, which is of the same order).

Table 8.3 - XRD results of combustion residues.

Identified Phases					
Propellant	Pressure (bar)	Al^0	γ Al_2O_3(%)	δ*Al_2O_3(%)	α Al_2O_3(%)
P_01a	1	3.6	56.7	37.4	2.4
P_01a	30	1.5	57.2	37.7	3.6
P_05	1	71.9	16.70	9.0	2.4
P_05	30	9.8	48.4	40.0	1.8

Secondly, although the flame temperature is well above the value requested to get the α form (≈1400 K), the transition aluminas γ and δ* found in all the samples and their relative abundance means that these temperatures have been experienced by the residues only for very short times. Furthermore, there should be a high temperature gradient between the burning surface of the propellant and the layers below, so that most part of aluminum oxidized is involved in a temperature range typical of transition aluminas γ and δ*.

Although the presence of the transition γ form is quite classic for such samples, the presence of δ* form requests a brief discussion. The δ* form is only reported in the paper of D. Forgeot et al [5], in which it is described as the only intermediate phase appearing during the γ to α transitions between 850° C and 1050 °C of plasma alumina sample sprayed and quenched in cold water.

The oxidation process of Al particles is very fast, starting at low temperature, going to high temperature until the quenching by the cooling jacket. All these formation processes occur in non-equilibrium thermodynamic conditions, and all the formed phases are likely frozen by the quenching procedure. This could reasonably explain the presence of both the metastable transition aluminas and low content of corundum found in all the samples.

8.5 Residues analysis conclusions

This Section summarizes the experimental data on residual oxide products formed during the combustion of propellants described in Sec. 5 (Tables 5.2 and 5.3). Attention was mainly focused on a physicochemical analysis of these residues, in order to investigate the effects produced by nano-aluminized propellants on condensed combustion products.

Interesting results have been found (such as the presence of γ and δ* matastable transition aluminas, effects of pressure, detailed chemical composition, and so on) but unfortunately the followed approach does not allow a direct answer on the general behavior of nano-aluminized propellants combustion products. In order to obtain this answer, the combustion behavior has to be studied at a micro scale; the physicochemical interaction involving the aluminum particles and the decomposition products both from the oxidizer and binder need to be investigated.

PART V CONCLUSIONS AND FUTURE WORK

9. CONCLUSIONS, OPEN QUESTIONS, AND FUTURE WORK

9.1 Conclusions

AP/HTPB-based aluminized composite solid rocket propellants, containing nanometric Al particles, show faster steady burning rates compared to the corresponding compositions containing micrometric Al particles. This increase is mainly determined by the intense energy released by ultra-fine particle oxidation closer to the burning surface and may be further supported by the higher propellant density. Nano-Al particles manifest a strong reactivity (equivalent to an increase of the premixed heat release contribution) mainly due to an increased specific surface (from 1.27 m^2/g of 17 μm Al to around 16 m^2/g of Alex) notwithstanding the simultaneous decrease of active Al content (from 99.6% of 17 μm Al to 88.2% of Alex). But probably this is accompanied by other effects as well. Burning rate is essentially not affected by particles in the micrometric range (say, $\geq$ 1 μm) but strongly increased by decreasing size particles in the nanometric range (say, 0.1-0.2 μm); the intermediate interval 0.2-1 μm needs more investigation. Within the limit of the carried out experimentation, pressure exponent is only subject to minor changes for commercial grade AP.

A global characterization has been carried out to compare different aluminum powders, from micro down to nano size. In all samples, although at different size, metallic-Al is dispersed as irregular regions (filaments, dots) inside Al-oxide particles. Chemical analysis confirmed that the passivation material for these powders is aluminum oxide, not always in stoichiometric ratio, which allows easy handling.

Considering in particular the three powders Al_01a (ultra fine, 0.1 μm), Al_03-d (fine, 2.5 μm), and Al_05 (coarse, 30 μm), Table 9.1 presents the measured steady burning rate obtained at 30 bar for the corresponding AP/HTPB propellants of the same composition (except the type of Al powder). It is shown that the replacement of the Al-powder μ-Al_05 with the powder n-Al_01 in the propellant manufacture increases burning rate of approximately 82 %. It can be also observed the increase of propellant density when the Al-powder nominal size decreases. Table 9.1 also includes XPS, XRD, and BET results for these powders.

Table 9.1 - Atomic concentration of total and metal Al per unit volume (by XPS), crystalline domain size (by XRD), burning rate, density, and BET specific surface of solid propellants manufactured using the indicated Al powders.

Al-powder	Nominal size, μm	Al-total Conc., [by XPS] at %	Al-metal Conc., [by XPS] at %	Al domain size, [by XRD] nm	Burning rate, [at 30 bar] mm/s	Propellant density, g/cm^3	BET specific surface, m^2/g
Al_05	30	92	84	200	5.22	1.52	<1
Al_03d	2.5	89	68	98	5.10	1.56	<1
Al_01a	0.1	64	38	130	9.52	1.67	15.6 ± 0.1

The Al particle size and distribution inside the propellant seem to be the fundamental parameters affecting the burning characteristics. The measured specific surface of Al_01a is around 15.6 m^2/g and thus much larger than that of Al_05 and Al_03d, both below the threshold limit of 1 m^2/g of the available ASAP 2010 instrument. Electron micrographs of pure powders, by *SEM* and *TEM*, showed a peculiar characteristic of Al_01a powder in comparison to others, pointing out a possible additional factor important for the increased burning rate: Al_01a is really fine dispersed at nanoscopic scale as a fractal structure. In particular, the Al_01a particle distribution appears is bimodal (Fig. 4.5a): larger particles of 200-300 nm are embedded in a multitude of smaller particles of 10-50 nm. These are mainly constituted by highly dispersed nano aluminum, passivated by amorphous Al-oxide and hence of spherical shape (Fig. 4.5c, 4.5d). In addition, some hexagonal particles are mixed to spherical ones (Fig. 4.5d, 4.5e); these are reasonably AlN, as found by

XRD, of about 20 nm of diameter, which represent the 3.5 % of the crystalline fraction. The possible role of AlN in determining good burning performance has to be further investigated.

At any rate, neither the Al total amount per unit volume nor the size of crystalline domains are responsible for the increased burning rate. *XPS* data show that n-Al_01 contains the lowest concentration of total aluminum and also the lowest concentration of metallic aluminum, per unit volume, as summarized in Table 9.1. The aluminum concentration is, instead, proportional to the particle prevailing dimension. The average crystalline domain lengths, as detected by *XRD,* were similar in the three samples (130 nm, 98 nm, and 200 nm, respectively), whatever the original particle dimension was. In the same way, the Al-metal amount per unit volume cannot be assumed as a good parameter to justify better performances of Al_01a powder. Thus, the large specific surface and fractal fine dispersion found in powder Al_01a only are the key points for the higher burning rate explanation.

9.2 Open questions

Interest in nano-sized metal particles is motivated by their applications in improving the current ballistic performance of solid, liquid, hybrid chemical rocket propulsion, monopropellant and gels systems, airbreathing systems in general (thanks to the decreased ignition delay of fuels). Use of nano-particles could favor the development of new technologies, such as cryogenic solids and water slurries in chemical rocket propulsion, colloid thrusters in electrical propulsion, increased thermal conductivity suspensions, etc.

Using nano-Al, the most common among nano-size ingredients, density and specific impulse are improved, while cost and safety aggravate. One major challenge with this technology is particle aggregation / agglomeration, in which the size of the metal particles respectively before / during combustion impacts various parts of the propulsive systems. Pre-burning aggregation (forming clots or lumps or clusters, typical of nano-Al) and burning agglomeration (typical of Al in general) are complex phenomena ultimately yielding an increase of the apparent metal particle size. This is detrimental for most performance parameters. Thus, in the current practice, nano-Al particles are coated with a protective layer to avoid “cold” (pre-burning) aggregation, surface oxidation, and inadvertent ignition; coatings can also be used to avoid “hot” (during burning) agglomeration. Friction, impact, and moderate temperature increase do not hinder handling of nano-Al, but electrostatic discharges may be risky.

For aluminized formulations containing nano-Al particles (say, below 0.2 μm), evidence from international laboratories has been collected for increased burning rate, decreased ignition delay, vigorous subatmospheric burning, reduced hot agglomeration, more efficient metal burning, decrease of flame heterogeneity, reduced specific impulse losses, and reduced[27] particulate damping especially at low pressures. The exact results depend on the many formulation details.

Among the many questions to be clarified:

- How does steady burn rate scale with specific surface?
- What chemical or physical factors contribute to the enhanced reactivity of nano-powders?
- What are the best coatings for nano particles?

(comments also reported – with editorial changes - in AIAA Aerospace America, Dec 04, pp. 62-63).

9.3 FUTURE WORK

As summarized by Dr. Chang, Director, US Army Research Office, combustion characteristics of conventional propellants are governed by characteristics of composite formulations:

- Multi-scale, multi-component: particulates plus binder
- Particulate size distributions lead to local non-uniformity and clustering of smaller components
- Significant aggregation of aluminum (if present) prior to ignition
- Rate of reaction limited by species and thermal diffusivity

A novel approach to propellant formulation and operation should promote:

- Reduced size dispersion
- Greater uniformity
- Reduce aggregation / agglomeration of aluminum
- Higher reaction rates

A radical approach to propellant formulation and operation might include:

- Controllable energy release

Nanoscale energetic materials may be the pathway to advanced energetic materials.

Again according to Dr. Chang, Director, US Army Research Office, the overall effort from an historical point of view may be conveniently classified as follows:

- 1st Generation (pre 2000)
Nanometer-sized Al powder/conventional propellants.
Some performance gain, variable results.

- 2nd Generation (current efforts)
Coated nanometer-sized metal powders.
Controlled oxidation, improved storage lifetime.
Quasi-ordered nanometer-sized inclusions in energetic matrix.
Cryo-Gel/Sol-Gel processing.

- 3rd Generation
3-dimensional nanoenergetics.
Structured/ordered.
Controlled reactivity.
Improved manufacturability/processing.

Use of nano-Al powders for solid rocket propellants appears feasible and advantageous. Yet several shortcomings exist, such as: hazards of handling, ageing during storage, compatibility with other ingredients, ignition and burning rate control, condensed combustion product size, effects on acoustic waves attenuation, etc. Several of these shortcomings could be either solved or substantially alleviated by a suitable coating of nano-Al powders. This first year of investigation was focused on uncoated nano-Al powders (first generation powders); next year of investigation will concentrate on coated nano-Al powders (second generation powders). A look at Table 1.1 will point out that at least 3 kinds of coated nano-Al from different Russian sources will be considered: type 04, 07, and 08.

PUBLICATIONS AND TECHNICAL REPORTS BASED ON THIS CONTRACT

1. L. Galfetti, F. Severini, G. Colombo, L.T. DeLuca, L. Meda, A. Vorozhtsov, V. Sedoi, V. Babuk, and B.N. Kondrikov, "Ballistic Properties of Nano-Aluminized High-Energy Materials (HEM)", Design, Test, Integration and Packaging of MEMS/MOEMS, DTIP 2004, Montreux, Switzerland, 12-14 May 2004.

2. L. Galfetti, F. Severini, L.T. DeLuca, and L. Meda, "Nano Propellants for Space Propulsion", Space Propulsion 2004, 4th International Spacecraft Propulsion Conference, Chia Laguna (Cagliari), Italy, 2-9 June 2004. Proceedings SP-555 of Space Propulsion 2004, ESA.

3. L.T. DeLuca, L. Galfetti, F. Severini, L. Meda, V.A. Babuk, B.N. Kondrikov, A.B. Vorozhtsov, and V. Sedoi, "Nano-Propellants for Aerospace Propulsion", International Symposium on Energy Conversion Fundamentals, Istanbul, Turkey, 21-25 Jun 04.

4. L. Galfetti, F. Severini, L.T. DeLuca, L. Meda, and V.A. Babuk, "Physical Characterization of Nanoaluminum Formulations", Zel'dovich Memorial II, Progress in Combustion and Detonation, Moscow, Russia, 30 August – 3 September 2004. Book of Abstracts, pp. 145-146.

5. L.T. DeLuca, L. Galfetti, F. Severini, L. Meda, B.N. Kondrikov, A. Vorozhtsov, and V. Sedoi, "Ballistic Properties of Nanoaluminized Solid Rocket Propellants", Zel'dovich Memorial II, Progress in Combustion and Detonation, Moscow, Russia, 30 August – 3 September 2004. Book of Abstracts, pp. 149-150.

6. L. Galfetti, L.T. DeLuca, F. Severini, F. Maggi, L. Meda, and G. Marra, "Characterization of Nano-Aluminum Powders for Solid Rocket Propellants", International Workshop HEMs-2004, High Energy Materials: Demilitarization and Civil Applications, Belokurikha, Biysk, 6-9 September 2004.

7. L. Meda, G. Marra, L. Galfetti, S. Inchingalo, F. Severini, and L.T. DeLuca, "Nano Composites for rocket solid propellants", CSTE, Composites Science and Technology, November 2004.

8. L. Meda , G.L. Marra, R. Braglia, L. Abis, R. Gallo, F. Severini, L. Galfetti, and L.T. DeLuca, "A Wide Characterization of Aluminum Powders for Propellants", Proceedings of the 9-IWCP, Novel Energetic Materials and Applications, November 2004, paper 17.

9. L. Galfetti, F. Severini, L.T. DeLuca, G. Marra, L. Meda, and R. Braglia, "Ballistics and Combustion Residues of Aluminized Solid Rocket Propellants", Proceedings of the 9-IWCP, Novel Energetic Materials and Applications, November 2004, paper 18.

10. D.A. Lucca, M.J. Klopfstein, O.R. Mejia, L. Rossettini, and L.T. DeLuca, "Investigation of the Near Surface Mechanical Properties of Ammonium Perchlorate using Nanoindentation", Proceedings of the 9-IWCP, Novel Energetic Materials and Applications, November 2004, paper 31.

11. V.A. Babuk, V.A. Vasilyev, A.A. Glebov, I.N. Dolotkazin, M. Galeotta, and L.T. DeLuca, "Combustion Mechanisms of AN-Based Aluminized Solid Rocket Propellants", Proceedings of the 9-IWCP, Novel Energetic Materials and Applications, November 2004, paper 44.

12. L.T. DeLuca, L. Galfetti, and R.A. Pesce-Rodriguez, Editors, "Novel Energetic Materials and Applications", Proceedings of the 9-IWCP, Grafiche GSS, Bergamo, Italy.

13. L.T. DeLuca, "New Energetic Ingredients for Improved Chemical Propulsion", Journée de travail *"Infrastructures spatiales et systèmes propulsifs"*, Toulouse, France, 01 Dec 04. Proceedings by ONERA, Jan 05.

LIST OF ALL PARTICIPATING SCIENTIFIC PERSONNEL

L.T. DeLuca, Professor
L. Galfetti, Professor
F. Severini, Professor

G. Colombo, Technician

F. Maggi, doctoral candidate
L. Rossettini, initially MSc. in Aerospace Engineering, now doctoral candidate
M. Saraswat, doctoral candidate

F. Campagnoli, initially MSc. in Aerospace Engineering, now completed
M. Donati, initially MSc. in Aerospace Engineering, now completed
C. Gallina, initially MSc. in Aerospace Engineering, now completed
S. Inchingalo, initially MSc. in Aerospace Engineering, now completed
N. Malheiro Da Silva, Erasmus exchange student, MSc., now completed
D. Orsini, MSc. in Aerospace Engineering
A. Piatti, initially MSc. in Aerospace Engineering, now completed
A. Salvagnin, initially MSc. in Aerospace Engineering, now completed

REFERENCES

[1] Mench, M.M., Yeh, C.L., and Kuo, K.K., "Propellant Burning Rate Enhancement and Thermal Behavior of Ultra-Fine Aluminum Powders (Alex)", Energetic Materials: Production, Processing and Characterization, Proceedings of the 29th International Annual Conference of ICT, 30-1-15, Karlsruhe, Federal Republic of Germany, 1998.

[2] Olivani, A., Galfetti, L., Severini, F., Colombo, G., Cozzi, F., Lesma, F., and Sgobba, M., " Aluminum Particle Size Influence on Ignition and Combustion of AP/HTPB/Al Solid Rocket Propellants", presented at RTO Specialist's Meeting on Advances in Rocket Propellant Performance, Life and Disposal for Improved System Performance and Reduced Costs, organized by the Members of the Applied Vehicle Tecnology Panel (AVT), Aalborg, Denmark, 23-26 September 2002.

[3] De Luca, L.T., Caveny, L.H., Ohlemiller, T.J., and Summerfield, M., "Radiative Ignition of Solid Propellants: I. Some Formulation Effects", AIAA Journal, Vol. 14, No. 7, pp. 940-946, 1976.

[4] DeLuca, L. T., Ohlemiller, T. J., Caveny, L. H., and Summerfield, M., "Radiative Ignition of Double-Base Propellants: II. Pre-Ignition Events and Source Effects," AIAA Journal, Vol. 14, No. 8, August 1976, pp. 1111-1117.

[5] Hermance, C.E., "Solid-Propellant Ignition Theories and Experiments", in "*Fundamentals of Solid Propellants Combustion*", edited by K.K. Kuo and M. Summerfield, Vol. 90, Chapter 5, AIAA Progress in Aeronautics and Astronautics, 1984.

[6] Lengellé, G., Bizot, A., Duterque, J., and Amiot, J., "Allumage des Propergols Solides", La Recherche Aérospatiale, pp. 1-20, 1991.

[7] Tepper, F., and Kaledin, L.A., "Combustion Characteristics of Kerosene Containing Alex Nano-Aluminum", Combustion of Energetic Materials, K.K. Kuo, L.T. DeLuca, Editors, Begell House, Inc., New York, Wallingford, 2002, pp. 195-206.

[8] Simonenko, V.N., and Zarko, V.E., "Comparative Study of the Combustion Behavior of Fine Aluminum", in "Energetic Materials", Proceedings of the 30th International Annual Conference of ICT, Karlsruhe, Germany, 1999, paper 21.

[9] Vorozhtsov, A.B., et al., "Ignition and Combustion of Solid and Gelled Propellants Containing Ultra-Fine Aluminum", in "Rocket Propulsion: Present and Future", edited by L.T. DeLuca, Grafiche GSS, Bergamo, Italy, 2003, paper 36.

[10] Price, E.W., "Combustion of Aluminum in Solid Propellant Flames", AGARD CP-259, 1979, paper 14.

[11] Price, E.W., "Combustion of Metalized Propellants", Fundamentals of Solid Propellants Combustion, edited by K.K. Kuo and M. Summerfield, Vol. 90, Progress in Aeronautics and Astronautics, AIAA, New York, 1984, pp. 478-513.

[12] Dreizin, E.L., "Experimental Study of Stages in Aluminum Combustion in Air", Combustion and Flame, Vol. 105, No. 4, 1996, pp. 541-556.

[13] Trubert, J.F., "Agglomeration and Combustion of Aluminum Particles in Solid Rocket Motors", Proceedings of the Space Solid Propulsion Workshop, Rome, 21-24 November 2000, paper 44.

[14] Melcher, J.C., Burton, R.L., and Krier, H., "Burning Aluminum Particles Inside a Laboratory Scale Solid Rocket Motor", AIAA 2001-3947, 37th AIAA/ASME/SAE/ASEE Joint Propulsion Conference and Exhibit, 2001.

[15] Shafirovich, E., Escot, P., Chauveau, C., Gökalp, I., Rosenband, V., and Gany, A., "Combustion of Single Aluminum Particles with Thin Nickel Coatings", in: *"Novel Energetic Materials and Applications"*, edited by L.T. DeLuca, L. Galfetti, and R.A. Pesce-Rodriguez, Grafiche GSS, Bergamo, Italy, 2004, paper 49.

[16] Dokhan, A., Seitzman, J.M., Price, E.W., and Sigman, R.K., "The Effects of Al Particle Size on the Burning Rate and Residual Oxide in Aluminized Propellants", AIAA Paper 2001-3581, 37th AIAA/ASME/SAE/ASEE Joint Propulsion Conference and Exhibit, Salt Lake City, UT, 8-11 July 2001.

[17] Dokhan, A., Price, E.W., Sigman, R.K., and Seitzman, J.M., "Combustion Mechanism of Bimodal and Ultra-fine Aluminum in AP Solid Propellant", AIAA Paper 2002-4173, 38th AIAA/ASME/SAE/ASEE Joint Propulsion Conference and Exhibit, Indianapolis, IN, 7-10 July 2002.

[18] Dokhan, A., Price, E.W., Seitzman, J.M., and Sigman, R.K., "The Ignition of Ultra-fine Aluminum in AP Solid Propellant Flames", AIAA Paper 2003-4810, 39th AIAA/ASME/SAE/ASEE Joint Propulsion Conference and Exhibit, Huntsville, AL, 20-23 July 2003.

[19] Price, E.W., and Sigman, R.K., "Combustion of Aluminized Solid Propellants", Solid Propellant Chemistry, Combustion, and Motor Interior Ballistics, AIAA Progress in Astronautics and Aeronautics, edited by V. Yang, T.B. Brill, W.Z. Ren, Vol. 185, 2000, pp. 663-687.

[20] Babuk, V.A., Belov, V.P., Khodosov, V.V., and Sheluken, G.G., "Investigation of the Agglomeration of Aluminum Particles During the Combustion of Metalized Condensed Systems", Fizika Goreniya I Vzryva, Vol. 21, No. 3, 1985, pp. 20-25.

[21] Babuk, V.A., Vassiliev, V.A., and Malakhov, M.S., "Condensed Combustion Products at the Burning Surface of Aluminized Solid Propellant", Journal of Propulsion and Power, Vol. 15, No. 6, 1999, pp. 783-793.

[22] Babuk, V.A., Vassiliev, V.A., and Sviridov, V.V., "Formation of Condensed Combustion Products at the Burning Surface of Solid Rocket Propellant", Solid Propellant Chemistry, Combustion, and Motor Interior Ballistics, AIAA Progress in Astronautics and Aeronautics, edited by V. Yang, T.B. Brill, W.Z. Ren, Vol. 185, 2000, pp. 749-776.

[23] Babuk, V.A., Vassiliev, V.A., and Sviridov, V.V., "Propellant Formulation Factors and Metal Agglomeration in Combustion of Aluminized Solid Rocket Propellant", Combustion Sci. and Tech., 2001, pp. 261-289.

[24] Babuk, V.A., and Vasilyev, V.A., "Model of Aluminum Agglomerate Evolution in Combustion Products of Solid Rocket Propellant", Journal of Propulsion and Power, Vol. 18, No. 4, 2002.

[25] Weiser, V., Eckl, W., Eisenreich, N., Kelzenberg, S., Plitzko, Y., Poller, S., and Roth, E., "Burning Behavior of Aluminized Composite Propellants Including Nanoparticles", in: *"Novel Energetic Materials and Applications"*, edited by L.T. DeLuca, L. Galfetti, and R.A. Pesce-Rodriguez, Grafiche GSS, Bergamo, Italy, 2004, paper 17.

[26] Bui, D.T., Atwood, A.I., and Atienza Moore, T.M., "Effect of Aluminum Particle Size on Combustion Behavior of Aluminized Propellants in PCP Binder", Proceedings of the 35th International Annual Conference of ICT, Karlsruhe, Germany, 2004, paper 27

[27] Arkhipov, V.A., et al., "Acoustic Admittance Function Study for Solid Propellants Containing Ultrafine Aluminum", in: *"Novel Energetic Materials and Applications"*, edited by L.T. DeLuca, L. Galfetti, and R.A. Pesce-Rodriguez, Grafiche GSS, Bergamo, Italy, 2004, paper 22.